Fermi National Accelerator Laboratory

FERMILAB-Pub-90/63-E
[E-537]

ψ Production in $\bar{p}N$ and π^-N Interactions at 125 GeV/c and a Determination of the Gluon Structure Functions of the $\bar{p}$ and the π^- *

S. Tzamarias, S. Katsanevas, C. Kourkoumelis, A. Markou, L. K. Resvanis, G. Voulgaris
University of Athens
Athens, Greece

M. Binkley, B. Cox, J. Enagonio, C. Hojvat, D. Judd, R. D. Kephart, P. K. Malhotra, P. O. Mazur, C. T. Murphy, F. Turkot, R. L. Wagner, D. E. Wagoner and W. Yang
Fermi National Accelerator Laboratory
P.O. Box 500
Batavia, Illinois 60510

H. Areti, S. Conetti, P. Lebrun, D. Ryan, T. Ryan, W. Schappert and D. G. Stairs
McGill University
Montreal, Quebec, Canada H3A 2T8

C. Akerlof, P. Kraushaar, D. Nitz and R. Thun
University of Michigan,
Ann Arbor, Michigan 48109

He Mao and Zhang Nai-jain
Shandong University
Jinan, People's Republic of China

April 1, 1990

* Submitted to Phys. Rev. D.

Operated by Universities Research Association Inc. under contract with the United States Department of Energy

Fermilab

Fermi National Accelerator Laboratory
P.O. Box 500 • Batavia, Illinois • 60510

ψ PRODUCTION IN $\bar{p}N$ AND π^-N INTERACTIONS AT 125 GeV/c AND A DETERMINATION OF THE GLUON STRUCTURE FUNCTIONS OF THE $\bar{p}$ AND THE π^-

April 1st., 1990

S. Tzamarias,[a] S. Katsanevas, C. Kourkoumelis, A. Markou,
L. K. Resvanis, G. Voulgaris,
University of Athens, Athens, Greece

M. Binkley, B. Cox,[b] J. Enagonio,[c] C. Hojvat, D. Judd,[d]
R. D. Kephart, P. K. Malhotra,[e] P. O. Mazur, C. T. Murphy, F. Turkot,
R. L. Wagner, D. E. Wagoner,[d] W. Yang,
Fermi National Accelerator Laboratory, Batavia, Illinois, USA 60510*

H. Areti,[c] S. Conetti,[b] P. Lebrun,[c] D. Ryan, T. Ryan,[f]
W. Schappert,[g] D. G. Stairs,
McGill University, Montreal, Quebec, Canada H3A 2T8

C. Akerlof, P. Kraushaar,[h] D. Nitz, R. Thun,
University of Michigan, Ann Arbor, Michigan, USA 48109

and

He Mao and Zhang Nai-jian
Shandong University, Jinan, People's Republic of China

Submitted to Physical Review D

PACS number: 13.85.Qk

* Operated by Universities Research Association Inc. under contract with the US Department of Energy.

(a) Present address: Northwestern University, Evanston, Illinois, USA.

(b) Present address: Univ. of Virginia, Charlottesville, Virginia, USA.

(c) Present address: Fermilab, Batavia, Illinois, USA.

(d) Present address: Prairie View A&M University, Prairie View, Texas, USA.

(e) Permanent address: Tata Institute, Bombay, India.

(f) Present address: Cornell University, Ithaca, New York USA.

(g) Present address: University of Chicago, Chicago, Illinois, USA.

(h) Present address: Shell Oil, Houston, Texas, USA.

ABSTRACT

We have measured the cross section for production of ψ and ψ' in $\bar{p}$ and π^- interactions with W, Cu and Be targets in the experiment E-537 at Fermilab. The measurement was performed at 125 GeV/c using a forward dimuon spectrometer in a closed geometry configuration. The gluon structure functions of the $\bar{p}$ and π^- have been extracted from the data from the measured $d\sigma/dx_F$ spectra of the produced ψ's. We obtain for the $\bar{p}$, averaged over all three targets:

$$xG(x) = (2.15 \pm 0.7)\ [1 - x]^{(6.83 \pm 0.5)}\ \ [1 + (5.85 \pm 0.95)x]$$

In the π^- case, we obtain:

$$xG(x) = (1.49 \pm 0.03)\ [1 - x]^{(1.98 \pm 0.06)} \qquad \text{from the } \pi^-\text{W data and}$$

$$xG(x) = (1.10 \pm 0.10)\ [1 - x]^{(1.20 \pm 0.2)} \qquad \text{from the } \pi^-\text{Be data.}$$

Introduction

A large fraction of the ψ hadroproduction cross section is thought to be due to "fusion" between the gluons in the beam hadron and the gluons in the target nucleus.[1] Because of this, ψ hadroproduction can be used to determine the gluon structure functions of the target nucleon and beam hadron, provided the production mechanisms involving those gluons are understood. However, any attempt to determine accurately these gluon structure functions requires knowledge of the quark structure functions of the interacting hadrons since some fraction of the production of ψ and ψ' is due to quark interactions. The quark structure functions of the nucleons have been independently measured in deep inelastic scattering experiments.[2] The pion quark structure functions must be determined through the study of hadronic processes and less data is available for this purpose. Furthermore, it is important in these studies, if large A nuclei are used, that corrections be made for the modified wave functions of quarks and gluons inside a heavy nucleus.[3,4]

This experiment, E-537,[5] has measured simultaneously the production of ψ, ψ' and the Drell-Yan dimuon continuum by antiprotons and pions on various nuclear targets at 125 GeV/c. We have determined the quark structure functions for both the $\bar{p}$ and π^- from the Drell-Yan measurements.[6] Use of quark structure functions determined in the same experiment minimizes the systematic errors in the computation of the gluon structure functions.

I. The Spectrometer

Experiment E-537 has measured the production of high mass dimuons using a tertiary 125 GeV/c $\bar{p}$ and π^- beam in the High Intensity Laboratory at Fermilab and a large aperture forward spectrometer.[5] The antiproton enriched beam produced by Λ^*, $\bar{\Lambda}^*$ and K_S^* decays contained 18% $\bar{p}$ and 82% π^-.

The spectrometer, described in detail elsewhere,[5] is shown in fig. 1. The apparatus included a W, Cu, or Be target, a Cu hadron absorber, a large aperture dipole analysis magnet, twenty proportional and drift multiwire chamber planes used as tracking elements, scintillation counter hodoscopes and a muon detector consisting of three planes of scintillation counters imbedded in 300 tons of steel and concrete.

The first level fast dimuon trigger required at least two three-fold coincidences among aligned counters in each of the three muon hodoscope planes, at least two hits in the charged particle hodoscope, and a $\bar{p}$ or π^- signal from the beam tagging system. Events which satisfied the fast trigger were then sent to a dedicated 2nd level ECL-CAMAC trigger processor[7] which kept only candidates with an effective mass greater than 2.0 GeV/c^2.

II. The Data Sample

The total data sample accumulated using the W target contained 12530 ψ events produced by the $\bar{p}$ beam and 33820 ψ events by the π^- beam. Figs. 2a and 2b show the effective mass distributions of the muon pairs along with Gaussian fits to the ψ and ψ' peaks plus the fit of an exponential function to the $\mu^+\mu^-$ continuum. In addition 529 ψ events from $\bar{p}$ Cu, 1958 from π^- Cu, 588 from $\bar{p}$ Be and 2881 from π^- Be interactions were collected. The mass resolution (σ = 180 MeV/c^2 for the W target, σ = 140 MeV/c^2 for the Cu target and σ = 200 MeV/c^2 for the Be target) was dominated by the target length and by the multiple scattering in the target and the Cu absorber.

Monte-Carlo simulations have been used to correct the data for geometric acceptances, hardware inefficiencies, re-interactions in the target, trigger processor inefficiency, vertex cut inefficiency, accidental coincidences and reconstruction inefficiencies[6]. The dependence of the cross section on the kinematical variables M, x_F, p_t, cosθ and ϕ have been extracted from the corrected data using a maximum likelihood technique as described in section IV of ref. 6b. As a check on the background subtraction, the mass spectrum has been fitted

in every bin of each of the other kinematical variables. The results obtained are in agreement with those obtained using the maximum likelihood method.

III. Differential and Total Cross Sections

In a previous paper[4] we have reported our measurement of the ψ production cross section in $\bar{p}$ and π^- interactions with W, Cu and Be targets. The A dependence of the π^- data for this experiment together with the H_2 and Pt results of NA3[8] can be described by the simple polynomial form:

$$\frac{\sigma_A}{A} = a + b\ A \qquad (1)$$

where σ_A is the total cross section (in nb/nucleus) at 125 GeV/c for a target with atomic number A. We obtained $a = 63.17 \pm 2.0$ and $b = -0.110 \pm 0.01$ from the fit to the π^- data. The same form (scaled down by 0.834 to account for the overall magnitude of the cross section) is also consistent with our $\bar{p}$ data. No hydrogen, or low A, data was available for an independent fit to the $\bar{p}$ data.

According to this parametrization (see ref. 9 for a possible phenomenological explanation), the total cross section per nucleon at 125 GeV/c is:

$$\begin{aligned} \sigma(\bar{p}\ N \to \psi + X) &= 52.59 \pm 1.7 \pm 3.15 \quad \text{nb/nucleon} \\ \sigma(\pi^- N \to \psi + X) &= 63.06 \pm 2.0 \pm 3.78 \quad \text{nb/nucleon} \end{aligned} \qquad (2)$$

The first error is due to the statistical uncertainty of the parametrization and the second error is due to the systematic uncertainty on the normalization of the experiment.

The ratio of the cross sections [continuum/ψ] has been measured and observed to vary with the target material as:

$$\begin{aligned} &0.103 \pm 0.02 \quad \text{for } \pi^- \text{ W} \\ &0.086 \pm 0.02 \quad \text{for } \pi^- \text{ Cu} \\ &0.065 \pm 0.02 \quad \text{for } \pi^- \text{ Be} \end{aligned} \tag{3}$$

The heavy ion experiment NA38[10] has observed that this ratio changes as a function of the total transverse energy per event. This effect has been interpreted as possible evidence for the formation of quark-gluon plasma. Our results indicate that this ratio may have a strong dependence on the atomic number of the target nucleus involved, which should be taken into account when inferences about the meaning of the heavy ion experiment are drawn.

The ratio of ψ' to ψ production for $\bar{p}$'s and π^-'s has been determined from our high statistics W target data. The observed ratios of the number of ψ and ψ' decaying into $\mu^+\mu^-$ are:

$$\frac{\psi' \to \mu^+\mu^-}{\psi \to \mu^+\mu^-} = 2.0\% \pm 1.0\% \quad \text{and} \quad 2.6\% \pm 0.7\% \tag{4}$$

for $\bar{p}$W and π^-W respectively. Correcting for the muon pair branching ratios of the ψ and ψ' we find:

$$\begin{aligned} &\frac{\sigma(\psi')}{\sigma(\psi)} = 18.50\% \pm 9.25\% \text{ for } \bar{p} \text{ W interactions.} \\ &\frac{\sigma(\psi')}{\sigma(\psi)} = 24.05\% \pm 6.50\% \text{ for } \pi^- \text{W interactions.} \end{aligned} \tag{5}$$

Using the ψ' inclusive cross section derived from these ratios and the measured branching ratio for the $\psi' \to \psi + X$ decay,[11] we find the fraction of the observed ψ coming from ψ' decay to be 9.8% ± 4.5% and 12.7% ± 3.5% for $\bar{p}$W and π^-W interactions respectively. This is consistent with the WA11[12] measurement in π^-Be interactions of 8% .

The differential cross sections $\frac{d\sigma}{dx_F}$, $\frac{d\sigma}{dp_t 2}$, $\frac{d\sigma}{d\cos\theta}$ and $\frac{d\sigma}{d\phi}$ for ψ production in π^-N interactions are presented in Tables 1a-c and in p^- interactions in Tables 2a-c.

Table 1a

π^- – W differential cross sections for ψ production in nb per W nucleus. The differential cross sections per nucleon (see text for scaling) are given in parenthesis. The scaling error of 3 % is not included in the Table.

x_F	$d\sigma/dx_F$ [nb/W nucleus]	[nb/nucleon]
0.025	16514.± 540.	(132.0±4.3)
0.075	17547.± 482.	(140.3±3.9)
0.125	16621.± 396.	(132.9±3.2)
0.175	16212.± 349.	(129.6±2.8)
0.225	15652.± 318.	(125.2±2.5)
0.325	12509.± 286.	(100.0±2.3)
0.375	11482.± 296.	(91.8±2.4)
0.425	9584.± 296.	(76.6±2.4)
0.475	7600.± 292.	(60.8±2.3)
0.525	6701.± 318.	(53.6±2.5)
0.575	4634.± 295.	(37.1±2.4)
0.625	3509.± 312.	(28.1±2.5)
0.675	2812.± 367.	(22.5±2.9)
0.725	1427.± 333.	(11.4±2.7)
0.775	602.± 270.	(4.8±2.2)
0.825	422.± 549.	(3.4±4.4)
0.875	474.± 893.	(3.8±7.1)
0.925	21.± 881.	(0.2±7.0)
0.975	0.± 93.	(0.0±0.7)

Table 1a - π^- W cont.

p_t^2	$d\sigma/dp_t^2$	
$(GeV/c)^2$	$[nb/(GeV/c)^2]$ per W nucleus	$[nb/(GeV/c)^2]$ per nucleon
0.225	5395.± 77.	(43.14±0.62)
0.675	3429.± 61.	(27.42±0.48)
1.125	2353.± 50.	(18.82±0.40)
1.575	1686.± 42.	(13.48±0.34)
2.025	1162.± 34.	(9.29±0.27)
2.475	868.± 30.	(6.94±0.24)
2.925	608.± 25.	(4.86±0.20)
3.375	459.± 21.	(3.67±0.17)
3.825	338.± 18.	(2.70±0.15)
4.275	282.± 17.	(2.26±0.14)
4.725	217.± 15.	(1.73±0.12)
5.175	160.± 13.	(1.28±0.10)
5.625	118.± 11.	(0.94±0.09)
6.075	97.± 10.	(0.78±0.08)
6.525	75.± 9.	(0.60±0.07)
6.975	63.± 8.	(0.50±0.06)
7.425	50.± 7.	(0.40±0.06)
7.875	42.± 7.	(0.34±0.05)
8.325	20.± 4.	(0.16±0.03)
8.775	25.± 5.	(0.20±0.04)

Table 1a - π^- W cont.

cos θ	$d\sigma/d\cos\theta$ [nb/W nucleus]	[nb/nucleon]
−0.95	4131.± 511.	(33.0±4.1)
−0.85	3976.± 272.	(31.8±2.2)
−0.75	3645.± 179.	(29.1±1.4)
−0.65	3715.± 149.	(29.7±1.2)
−0.55	3791.± 132.	(30.3±1.1)
−0.45	3893.± 123.	(31.1±1.0)
−0.35	3849.± 115.	(30.8±0.9)
−0.25	3971.± 112.	(31.7±0.9)
−0.15	4028.± 111.	(32.2±0.9)
−0.05	3898.± 106.	(31.2±0.8)
0.05	3891.± 106.	(31.1±0.8)
0.15	3824.± 107.	(30.6±0.9)
0.25	3969.± 114.	(31.7±0.9)
0.35	3905.± 117.	(31.2±0.9)
0.45	3937.± 124.	(31.5±1.0)
0.55	3880.± 135.	(31.0±1.1)
0.65	4161.± 163.	(33.3±1.3)
0.75	3816.± 181.	(30.5±1.4)
0.85	3982.± 257.	(31.8±2.1)
0.95	3835.± 416.	(30.7±3.3)

Table 1a - π^- W cont.

ϕ(deg.)	$d\sigma/d\phi$ [nb/W nucleus]	[nb/nucleon]
9.0	22.6±0.89	(0.181±0.007)
27.0	22.5±0.89	(0.180±0.007)
45.0	21.4±0.77	(0.171±0.006)
63.0	22.2±0.77	(0.178±0.006)
81.0	22.5±0.77	(0.180±0.006)
99.0	20.3±0.64	(0.162±0.005)
117.0	23.0±0.77	(0.184±0.006)
135.0	23.1±0.77	(0.185±0.006)
153.0	21.3±0.77	(0.170±0.006)
171.0	23.7±0.89	(0.190±0.007)
189.0	23.2±0.89	(0.186±0.007)
207.0	20.8±0.77	(0.166±0.006)
225.0	21.4±0.77	(0.171±0.006)
243.0	21.1±0.64	(0.168±0.005)
261.0	19.9±0.64	(0.159±0.005)
279.0	20.8±0.64	(0.166±0.005)
297.0	21.1±0.64	(0.168±0.005)
315.0	22.0±0.77	(0.176±0.006)
333.0	20.9±0.77	(0.167±0.006)
351.0	22.6±0.89	(0.181±0.007)

TABLE 1b

π^- – Cu differential cross sections for ϕ production in nb per Cu nucleus. The differential cross sections per nucleon (see text for scaling) are given in parenthesis. The scaling error of 4 % is not included in the Table.

x_F	$d\sigma/dx_F$ [nb/Cu nucleus]	[nb/nucleon]
0.050	7110.± 470.	(124.4± 8.2)
0.150	7669.± 371.	(134.2± 6.5)
0.250	5632.± 285.	(98.5± 5.0)
0.350	5173.± 295.	(90.5± 5.2)
0.450	4137.± 323.	(72.4± 5.7)
0.550	3034.± 380.	(53.1± 6.7)
0.650	1909.± 461.	(33.4± 8.1)
0.750	1297.± 813.	(22.7±14.2)
0.850	0.± 760.	(0.0±13.3)
0.950	0.±1045.	(0.0±18.3)

p_t^2	$d\sigma/dp_t^2$	
$(GeV/c)^2$	$[nb/(GeV/c)^2]$ per Cu nucleus	$[nb/(GeV/c)^2]$ per nucleon
0.450	1983.± 70.	(34.70±1.23)
1.350	856.± 45.	(14.99±0.79)
2.250	478.± 34.	(8.36±0.60)
3.150	206.± 22.	(3.60±0.38)
4.050	117.± 16.	(2.06±0.29)
4.950	62.± 12.	(1.09±0.20)
5.850	45.± 10.	(0.79±0.18)
6.750	12.± 5.	(0.22±0.09)
7.650	12.± 5.	(0.21±0.09)
8.550	14.± 7.	(0.24±0.11)

Table 1b - π^- Cu cont.

$\cos\theta$	$d\sigma/d\cos\theta$ [nb/Cu nucleus]	[nb/nucleon]
−0.90	1302.± 280.	(22.8± 4.9)
−0.70	1646.± 162.	(28.8± 2.8)
−0.50	1516.± 119.	(26.5± 2.1)
−0.30	1696.± 114.	(29.7± 2.0)
−0.10	1692.± 109.	(29.6± 1.9)
0.10	1839.± 114.	(32.2± 2.0)
0.30	1587.± 109.	(27.8± 1.9)
0.50	1658.± 128.	(29.0± 2.2)
0.70	1901.± 185.	(33.3± 3.2)
0.90	2048.± 375.	(35.8± 6.6)

ϕ(deg.)	$d\sigma/d\phi$ [nb/Cu nucleus]	[nb/nucleon]
18.0	10.1±0.86	(0.176±0.015)
54.0	9.6±0.75	(0.168±0.013)
90.0	8.7±0.66	(0.152±0.011)
126.0	10.1±0.76	(0.177±0.013)
162.0	10.3±0.86	(0.180±0.015)
198.0	9.4±0.82	(0.165±0.014)
234.0	9.6±0.75	(0.167±0.013)
270.0	9.6±0.68	(0.167±0.012)
306.0	8.3±0.69	(0.146±0.012)
342.0	9.2±0.83	(0.161±0.014)

TABLE 1c

π^- − Be differential cross sections for ψ production in nb per Be nucleus. The differential cross sections per nucleon (see text for scaling) are given in parenthesis. The scaling error of 4.5 % is not included in the Table.

x_F	$d\sigma/dx_F$ [nb/Be nucleus]	[nb/nucleon]
0.050	1030.± 67.	(116.2± 7.5)
0.150	1049.± 51.	(118.3± 5.7)
0.250	912.± 42.	(102.9± 4.7)
0.350	861.± 44.	(97.1± 5.0)
0.450	642.± 46.	(72.5± 5.1)
0.550	442.± 53.	(49.9± 6.0)
0.650	333.± 74.	(37.5± 8.4)
0.750	180.± 133.	(20.3±15.0)
0.850	116.± 158.	(13.1±17.9)
0.950	0.± 131.	(0.0±14.8)

p_t^2	$d\sigma/dp_t^2$	
$(GeV/c)^2$	$[nb/(GeV/c)^2]$ per Be nucleus	$[nb/(GeV/c)^2]$ per nucleon
0.450	332.± 11.	(37.44±1.19)
1.350	120.± 6.	(13.49±0.70)
2.250	61.± 4.	(6.87±0.50)
3.150	28.± 3.	(3.11±0.33)
4.050	14.± 2.	(1.57±0.23)
4.950	10.± 2.	(1.17±0.21)
5.850	5.± 1.	(0.57±0.14)
6.750	5.± 1.	(0.58±0.14)
7.650	2.± 1.	(0.18±0.09)
8.550	1.± 1.	(0.14±0.08)

Table 1c - π^- Be cont.

$\cos\theta$	$d\sigma/d\cos\theta$ [nb/Be nucleus]	$d\sigma/d\cos\theta$ [nb/nucleon]
−0.90	226.± 44.	(25.5± 5.0)
−0.70	260.± 24.	(29.3± 2.7)
−0.50	232.± 17.	(26.1± 1.9)
−0.30	270.± 16.	(30.5± 1.8)
−0.10	254.± 15.	(28.7± 1.7)
0.10	270.± 16.	(30.5± 1.8)
0.30	286.± 17.	(32.2± 1.9)
0.50	257.± 19.	(28.9± 2.1)
0.70	242.± 23.	(27.3± 2.6)
0.90	175.± 35.	(19.7± 3.9)

ϕ(deg.)	$d\sigma/d\phi$ [nb/Be nucleus]	$d\sigma/d\phi$ [nb/nucleon]
18.0	1.5±0.12	(0.173±0.014)
54.0	1.4±0.11	(0.159±0.012)
90.0	1.4±0.10	(0.159±0.011)
126.0	1.3±0.10	(0.151±0.011)
162.0	1.4±0.12	(0.158±0.013)
198.0	1.6±0.12	(0.180±0.014)
234.0	1.4±0.10	(0.157±0.011)
270.0	1.5±0.10	(0.174±0.011)
306.0	1.3±0.10	(0.148±0.011)
342.0	1.6±0.12	(0.175±0.014)

Table 2a

$\bar{p}$ − W differential cross sections for ψ production in nb per W nucleus. The differential cross sections per nucleon (see text for scaling) are given in parenthesis. The scaling error of 3.5 % is not included in the Table.

x_F	$d\sigma/dx_F$ [nb/W nucleus]	[nb/nucleon]
0.025	24262.± 974.	(185.3±7.4)
0.075	22578.± 792.	(172.4±6.0)
0.125	20178.± 646.	(154.1±4.9)
0.175	16566.± 527.	(126.5±4.0)
0.225	14473.± 465.	(110.5±3.6)
0.275	11624.± 403.	(88.8±3.1)
0.325	8043.± 326.	(61.4±2.5)
0.375	6435.± 301.	(49.1±2.3)
0.425	4401.± 260.	(33.6±2.0)
0.475	2946.± 221.	(22.5±1.7)
0.525	2004.± 199.	(15.3±1.5)
0.575	1114.± 158.	(8.5±1.2)
0.625	705.± 127.	(5.4±1.0)
0.675	388.± 101.	(3.0±0.8)
0.725	160.± 68.	(1.2±0.5)
0.775	167.± 105.	(1.3±0.8)
0.825	19.± 22.	(0.1±0.2)
0.875	28.± 42.	(0.2±0.3)
0.925	0.± 41.	(0.0±0.3)
0.975	0.± 13.	(0.0±0.1)

Table 2a - $\bar{p}$ W cont.

p_t^2	$d\sigma/dp_t^2$	
$(GeV/c)^2$	$[nb/(GeV/c)^2]$ per W nucleus	$[nb/(GeV/c)^2]$ per nucleon
0.225	5132.± 107.	(39.19±0.81)
0.675	3222.± 84.	(24.60±0.64)
1.125	2077.± 66.	(15.86±0.50)
1.575	1432.± 54.	(10.93±0.42)
2.025	1022.± 47.	(7.81±0.36)
2.475	724.± 38.	(5.53±0.29)
2.925	521.± 33.	(3.98±0.25)
3.375	348.± 26.	(2.65±0.20)
3.825	263.± 23.	(2.01±0.18)
4.275	201.± 20.	(1.54±0.15)
4.725	125.± 16.	(0.95±0.12)
5.175	79.± 12.	(0.60±0.09)
5.625	75.± 12.	(0.57±0.09)
6.075	81.± 13.	(0.61±0.10)
6.525	54.± 11.	(0.41±0.09)
6.975	42.± 10.	(0.32±0.08)
7.425	35.± 9.	(0.27±0.07)
7.875	19.± 6.	(0.15±0.05)
8.325	14.± 6.	(0.11±0.04)
8.775	18.± 6.	(0.13±0.05)

Table 2a - $\bar{p}$ W cont.

cos θ	$d\sigma/d\cos\theta$ [nb/W nucleus]	[nb/nucleon]
−0.95	3704.± 830.	(28.3±6.3)
-0.85	2870.± 345.	(21.9±2.6)
−0.75	3158.± 255.	(24.1±1.9)
−0.65	3464.± 221.	(26.4±1.7)
−0.55	3278.± 176.	(25.0±1.3)
−0.45	3657.± 153.	(27.9±1.2)
−0.35	3478.± 153.	(26.6±1.2)
−0.25	3440.± 153.	(26.3±1.2)
−0.15	3406.± 153.	(26.0±1.2)
−0.05	3441.± 153.	(26.3±1.2)
0.05	3653.± 153.	(27.9±1.2)
0.15	3773.± 153.	(28.8±1.2)
0.25	3446.± 153.	(26.3±1.2)
0.35	3600.± 153.	(27.5±1.2)
0.45	3511.± 153.	(26.8±1.2)
0.55	3446.± 186.	(26.3±1.4)
0.65	3152.± 208.	(24.1±1.6)
0.75	3496.± 280.	(26.7±2.1)
0.85	3688.± 393.	(28.2±3.0)
0.95	3752.± 676.	(28.7±5.2)

Table 2a - $\bar{p}$ W cont.

ϕ(deg.)	$d\sigma/d\phi$ [nb/W nucleus]	[nb/nucleon]
9.0	19.7±1.15	(0.150±0.009)
27.0	19.3±1.15	(0.147±0.009)
45.0	19.1±1.02	(0.146±0.008)
63.0	19.9±1.02	(0.152±0.008)
81.0	19.3±1.02	(0.147±0.008)
99.0	18.8±0.89	(0.143±0.007)
117.0	20.4±1.02	(0.156±0.008)
135.0	19.7±1.15	(0.150±0.009)
153.0	21.6±1.28	(0.165±0.010)
171.0	20.2±1.15	(0.154±0.009)
189.0	19.4±1.15	(0.148±0.009)
207.0	19.8±1.15	(0.151±0.009)
225.0	19.8±1.02	(0.151±0.008)
243.0	18.3±1.02	(0.139±0.008)
261.0	17.4±0.89	(0.133±0.007)
279.0	17.9±0.89	(0.136±0.007)
297.0	19.0±1.02	(0.145±0.008)
315.0	17.9±1.02	(0.136±0.008)
333.0	19.7±1.15	(0.150±0.009)
351.0	19.0±1.15	(0.145±0.009)

TABLE 2b

$\bar{p}$ − Cu differential cross sections for ψ production in nb per Cu nucleus. The differential cross sections per nucleon (see text for scaling) are given in parenthesis. The scaling error of 5 % is not included in the Table.

x_F	$d\sigma/dx_F$ [nb/Cu nucleus]	[nb/nucleon]
0.050	9694.± 996.	(181.1±18.6)
0.150	8730.± 732.	(163.1±13.7)
0.250	5040.± 498.	(94.2± 9.3)
0.350	3022.± 421.	(56.4± 7.9)
0.450	1727.± 394.	(32.3± 7.4)
0.550	597.± 315.	(11.2± 5.9)
0.650	0.± 0.	(0.0± 0.0)
0.750	0.± 0.	(0.0± 0.0)
0.850	0.± 0.	(0.0± 0.0)
0.950	0.± 0.	(0.0± 0.0)

p_t^2	$d\sigma/dp_t^2$	
$(GeV/c)^2$	$[nb/(GeV/c)^2]$ per Cu nucleus	$[nb/(GeV/c)^2]$ per nucleon
0.450	1931.± 125.	(36.08±2.33)
1.350	682.± 72.	(12.75±1.35)
2.250	338.± 50.	(6.32±0.94)
3.150	126.± 30.	(2.36±0.56)
4.050	101.± 27.	(1.90±0.51)
4.950	56.± 19.	(1.04±0.36)
5.850	7.± 10.	(0.14±0.19)
6.750	14.± 10.	(0.27±0.19)
7.650	6.± 12.	(0.12±0.22)
8.550	6.± 9.	(0.11±0.17)

Table 2b - $\bar{p}$ Cu cont.

cos θ	$d\sigma/d\cos\theta$ [nb/Cu nucleus]	[nb/nucleon]
−0.90	950.± 461.	(17.8± 8.6)
−0.70	1382.± 285.	(25.8± 5.3)
−0.50	1226.± 195.	(22.9± 3.6)
−0.30	1387.± 181.	(25.9± 3.4)
−0.10	1696.± 185.	(31.7± 3.5)
0.10	1601.± 185.	(29.9± 3.5)
0.30	1744.± 204.	(32.6± 3.8)
0.50	1387.± 209.	(25.9± 3.9)
0.70	1140.± 257.	(21.3± 4.8)
0.90	1041.± 466.	(19.4± 8.7)

ϕ(deg.)	$d\sigma/d\phi$ [nb/Cu nucleus]	[nb/nucleon]
18.0	7.9±1.38	(0.147±0.026)
54.0	8.6±1.28	(0.161±0.024)
90.0	8.0±1.14	(0.149±0.021)
126.0	9.5±1.38	(0.178±0.026)
162.0	8.6±1.43	(0.162±0.027)
198.0	8.0±1.38	(0.149±0.026)
234.0	8.2±1.24	(0.153±0.023)
270.0	6.8±1.05	(0.128±0.020)
306.0	7.2±1.19	(0.134±0.022)
342.0	9.0±1.43	(0.169±0.027)

TABLE 2c

$\bar{p}$ – Be differential cross sections for ψ production in nb per Be nucleus. The differential cross sections per nucleon (see text for scaling) are given in parenthesis. The scaling error of 5 % is not included in the Table.

x_F	$d\sigma/dx_F$ [nb/Be nucleus]	$d\sigma/dx_F$ [nb/nucleon]
0.050	1699.± 189.	(193.7±21.6)
0.150	1289.± 127.	(147.0±14.5)
0.250	891.± 90.	(101.7±10.3)
0.350	472.± 65.	(53.9± 7.4)
0.450	242.± 49.	(27.6± 5.6)
0.550	120.± 36.	(13.7± 4.1)
0.650	48.± 31.	(5.5± 3.5)
0.750	38.± 28.	(4.4± 3.2)
0.850	72.± 87.	(8.2±10.0)
0.950	0.± 7.	(0.0± 0.8)

p_t^2 $(GeV/c)^2$	$d\sigma/dp_t^2$ $[nb/(GeV/c)^2]$ per Be nucleus	$[nb/(GeV/c)^2]$ per nucleon
0.450	309.± 21.	(35.26±2.37)
1.350	127.± 13.	(14.45±1.51)
2.250	62.± 9.	(7.04±1.03)
3.150	17.± 5.	(1.99±0.54)
4.050	10.± 4.	(1.11±0.41)
4.950	4.± 3.	(0.47±0.36)
5.850	5.± 2.	(0.53±0.27)
6.750	0.± 2.	(0.00±0.21)
7.650	0.± 2.	(0.00±0.22)
8.550	1.± 2.	(0.08±0.21)

Table 2c - $\bar{p}$ Be cont.

$\cos\theta$	$d\sigma/d\cos\theta$ [nb/Be nucleus]	[nb/nucleon]
−0.90	195.± 99.	(22.2±11.3)
−0.70	227.± 49.	(25.9± 5.6)
−0.50	242.± 37.	(27.6± 4.2)
−0.30	249.± 32.	(28.4± 3.7)
−0.10	236.± 29.	(26.9± 3.3)
0.10	287.± 32.	(32.7± 3.7)
0.30	246.± 32.	(28.0± 3.7)
0.50	232.± 37.	(26.4± 4.2)
0.70	209.± 47.	(23.9± 5.4)
0.90	186.± 65.	(21.2± 7.4)

ϕ(deg.)	$d\sigma/d\phi$ [nb/Be nucleus]	[nb/nucleon]
18.0	1.5±0.25	(0.174±0.028)
54.0	1.3±0.21	(0.147±0.024)
90.0	1.1±0.18	(0.123±0.020)
126.0	1.5±0.22	(0.176±0.026)
162.0	1.3±0.23	(0.146±0.026)
198.0	1.1±0.21	(0.130±0.024)
234.0	1.5±0.22	(0.169±0.026)
270.0	1.5±0.21	(0.167±0.024)
306.0	1.3±0.21	(0.151±0.024)
342.0	1.2±0.22	(0.141±0.026)

IV. Comparison of the $\bar{p}$ data to the Semi-Local Duality Model

The differential cross section $d\sigma/dx_F$ for direct charmonium production in hadron-hadron interactions is given by:[13]

$$\frac{d\sigma}{dx_F} = \int dx_1 dx_2 \, \hat{\sigma}_{ij} \, \frac{(1-\tau)}{s(x_1+x_2)} \, f_i(x_1) \, f_j(x_2) \qquad (6)$$

where $\hat{\sigma}_{ij}$ is the partonic cross section for the fusion of the partons i and j into ψ

$\frac{1-\tau}{s(x_1+x_2)}$ is the usual kinematical factor, with s the centre of mass energy squared, x_1 and x_2 are the Bjorken variables and $\tau = Q^2/s$ is the momentum transfered squared.

$f_i(x)$, $f_j(x)$ are the parton i or j distribution functions of the interacting hadrons

For a particular partonic interaction (quark-quark, gluon-gluon or quark-gluon) the shape of the differential cross section $d\sigma/dx_F$ depends to a large degree on the convolution of the distribution functions

$$\frac{[f_i(x_1)f_j(x_2) + f_i(x_2)f_j(x_1)]}{(x_1 + x_2)} \qquad (7)$$

and is not sensitive to the choice of the model for charmonium production. Due to the fact that several partonic interactions contribute to charmonium hadroproduction, the shape of $d\sigma/dx_F$ depends on the relative strength of the individual partonic cross sections.

For the purpose of extracting the gluon extraction function we have used the semi local duality model (SLDM)[14], which contains quark-antiquark and gluon-gluon fusion, to provide us with a phenomenological framework. We have assumed that the SLDM describes the production of all the charmonium states. The specific prediction of the SLDM is:

$$\frac{d\sigma}{dx_F} = N \int_{4M_c^2}^{4M_D^2} dM^2 \left[\frac{\hat{\sigma}_{gg}(M^2,A^2)\ (1-\tau)\ G_1(x_1)\ G_2(x_2)}{s\ (x_1+x_2)} + \right. \tag{8a}$$

$$\left. + \frac{\hat{\sigma}_{q\bar{q}}(M^2,A^2)\ (1-\tau)}{s\ (x_1+x_2)} \sum_{k=1}^{n} f_k(x_1)\ \bar{q}_k(x_2) + \bar{f}_k(x_1)\ q_k(x_2) \right]$$

where M is the invariant mass of the $c\bar{c}$ pair, M_c and M_D are the charm quark and D-meson masses respectively, N is the fixed fraction of the $c\bar{c}$ production cross-section leading to a particular charmonium state, $x_1(x_2)$ is the fraction of the momentum of the beam (target) hadron which is carried by the parton and is given by:

$$x_{1,2} = 0.5 \left[\sqrt{x_F^2\ (1-\tau)^2 + 4\tau} \pm x_F(1-\tau) \right] \tag{8b}$$

$\tau = M^2/s = x_1x_2$ is the scaling variable, $G_1(x)$ and $G_2(x)$ are the gluon distribution functions, $f_k(x)$, $q_k(x)$ are the quark distribution functions and $\hat{\sigma}_{q\bar{q}}$, $\hat{\sigma}_{gg}$ are the point-like cross sections for the subprocess $q\bar{q} \rightarrow c\bar{c}$ and $gg \rightarrow c\bar{c}$ with:

$$\hat{\sigma}_{gg} = \frac{\pi\,\alpha_s^2}{3\,M^6}\left[\,(M^4 + 4\,M^2\,M_c^2 + M_c^4)\,\ln\!\left(\frac{M^2+\lambda}{M^2-\lambda}\right) - (7M^2 + 31M_c^2)\,\frac{\lambda}{4}\,\right]$$

$$\hat{\sigma}_{q\bar{q}} = \frac{8\pi\alpha_s^2}{27\,M^6}\,[M^2 + 2\,M_c^2\,]\,\lambda \qquad (8c)$$

$$\lambda^2 = M^4 - 4\,M^2M_c^2$$

with α_s being the coupling constant.

The ψ is either produced directly or as the decay product of the ψ' or the χ's. We have ignored the small fraction of ψ's that come from ψ' production and decay. The fraction of ψ's produced via χ decay in proton-proton interactions has been measured at the ISR by experiment R806[15] ($\sqrt{s}$ = 62 GeV) to be 0.47 ± 0.08, and a similar value of 0.47 ± 0.23 was obtained at Fermilab by experiment E673[16] ($\sqrt{s}$ = 18.9 GeV) in pBe interactions. No measurement has been published for ψ's produced in antiproton-nucleon interactions, so a value consistent with the proton results was used in the analysis.

The following analytical formula[17] gives the $d\sigma/dx_F$ distribution of the indirectly produced ψ's as a function of the $d\sigma/dx_F$ of the parent χ state.

$$\left.\frac{d\sigma}{dx_F}\right|_{\chi \to \psi} = \int_{a_1}^{a_2} \left.\frac{d\sigma}{dx_F}\right|_{\chi} \frac{M_\chi^2}{(M_\chi^2 - M_\psi^2)}\,\frac{(1-\tau_\psi)}{(x_1+x_2)_\chi}\,\left.dx_F\right|_{\chi} \qquad (9)$$

where:

$\left.\frac{d\sigma}{dx_F}\right|_{\chi \to \psi}$ is the observed x_F distribution of ψ from $\chi \to \psi + \gamma$ decays

$\left.\frac{d\sigma}{dx_F}\right|_{\chi}$ is the x_F distribution of the given χ state

M_χ , M_ψ are the masses of the χ and ψ mesons

$$a_{1,2} = 0.5\ x_F\Big|_\psi \frac{(1-\tau_\psi)}{(1-\tau_\chi)} \frac{(M_\chi^2 + M_\psi^2)}{M_\psi^2} \begin{matrix} - \\ + \end{matrix}$$

$$\begin{matrix} - \\ + \end{matrix} \frac{[(x_F)\Big|_\psi^2 (1-\tau_\psi)^2 + 4\tau_\psi]^{1/2}}{(1-\tau_\chi)} \frac{(M_\chi^2 - M_\psi^2)}{M_\psi^2}$$

with $\tau_\psi = M_\psi^2/s$ and $\tau_\chi = M_\chi^2/s$. We have assumed that in the rest frame of the χ, the azimuthal and $\cos\theta$ distributions of the photon are uniform (where θ is the angle between the photon direction and the beam axis). This prediction of the x_F distribution of the indirectly produced ψ's can be combined with the x_F distribution of the directly produced ψ's to get the $d\sigma/dx_F$ of the total ψ sample by:

$$\left.\frac{d\sigma}{dx_F}\right|_{observed} = \left[\ 1-w\ \right] \left[\ \frac{d\sigma}{dx_F}\ \right]_{direct\ \psi} + w \left[\ \frac{d\sigma}{dx_F}\ \right]_{\chi \to \psi} \qquad (10)$$

where w is the fraction of ψ's coming from the decay of the χ states.

The resulting prediction of $d\sigma/dx_F$ for the measured ψ production is used to extract the gluon structure functions from our data using w = 0.47. Varying the value of w from 0.3 to 0.47 (a range that includes the measured ratios in proton interactions quoted above and those for π^- interactions quoted in section VI below) changes the extracted structure function parameters by less than 2%. The x_F distribution of the indirectly produced ψ's is also found to be insensitive to the p_t distribution of the parent χ or to the angular distribution of the photon in the $\chi \to \psi + \gamma$ decay.

The Duke and Owens set 1 quark structure functions for the nucleon[18] (DO set 1) describes well our Drell-Yan data[6] for $\langle Q^2 \rangle = 25\ (GeV/c^2)^2$. We have used these structure functions with the SLDM and find that the Q^2 dependence of the structure function within our limits of integration $4M_c^2 < M^2 < 4M_D^2$ is not strong. Therefore, we fix $Q^2 = M_{c\bar{c}}^2$ and ignore the evolution of the structure functions with Q^2. The choice of the value of the parameter Λ and the mass of the charmed quark affect only the overall normalization and not the shape of the $d\sigma/dx_F$ spectra.

We have fitted the x_F distribution of the ψ's from our $\bar{p}W$ data using the SLDM prediction (eqs. 8 and 10) with the DO set 1 quark and gluon structure functions determined at $Q^2 = M_\psi^2$ leaving the overall normalization free. A value of $N = 0.188 \pm 0.002$ is found. Fig. 3 shows the excellent agreement (χ^2 per degree of freedom equal 1.0) between the fit and the data. From the results of this fit we estimate that 48% of ψ's are produced through gluon-gluon fusion.

We can also write the prediction of the SLDM for the ratio of the $\bar{p}$-nucleon to p-nucleon total ψ production cross sections at a particular $\sqrt{s}$ as:

$$R\ (\sqrt{s};\ \bar{p},p) = \frac{\left[\ \sigma^{\bar{p}}_{q\bar{q}}\ (\sqrt{s}) + \sigma^{\bar{p}}_{gg}\ (\sqrt{s})\ \right]}{\left[\ \sigma^{p}_{q\bar{q}}\ (\sqrt{s}) + \sigma^{p}_{gg}\ (\sqrt{s})\ \right]} \qquad (11)$$

where $\sigma^h_{q\bar{q}}$ (σ^h_{gg}) is the integral over x_F of the $q\bar{q}$ (gg) part of eq. 8 and h denotes the beam hadron. In ref. 4 we found that the dependence of the ψ production cross section on the atomic number is similar for $\bar{p}$ and π^- beams. Providing the same is true for proton-nucleus interactions, then the ratio R should be approximately independent of the specific target nucleus. In Table 3 we summarize the cross section ratio $R(\sqrt{s};\bar{p},\ p)$ for ψ production with antiproton and proton beams on nuclear targets at different beam energies.

TABLE 3

Cross section ratio for ψ production by $\bar{p}$'s and p's on nuclear targets at different energies. For E537 we have used the Lyons[20] parametrization for pN interactions as a function of $\sqrt{\tau}$ to estimate the cross section for ψ production by protons.

Experiment	Beam Momentum (GeV/c)	$\sqrt{s}$ (GeV/c^2)	$R(\sqrt{s};\bar{p},p)$
Ω (Ref. 19)	39.5	8.6	5.26 ± 0.83
E-537	125.0	15.3	2.0 ± 0.3
NA3 (Ref. 8)	150.0	16.8	2.35 ± 0.3
NA3 (Ref. 8)	200.0	19.4	1.46 ± 0.25

We have checked the possibility that there may be a relative normalization of the $q\bar{q}$ and gg processes (beyond the expectation of the simple SLDM) by fitting the variation of the ratio R as a function of $\sqrt{s}$ with two different normalization factors, $N_{q\bar{q}}$ and N_{gg}:

$$R(\sqrt{s};\ \bar{p},p) = \frac{\sigma^{\bar{p}}_{q\bar{q}}\ (\sqrt{s}) + K\ \sigma_{gg}\ (\sqrt{s})}{\sigma^{p}_{q\bar{q}}\ (\sqrt{s}) + K\ \sigma_{gg}\ (\sqrt{s})} \qquad \text{with} \quad K = \frac{N_{gg}}{N_{q\bar{q}}} \qquad (12)$$

Fitting eq. 12 to the data of Table 3 and using the DO set 1 structure functions for quarks and gluons, we obtain a value of K = 1.08 * 0.3. Therefore, we have fixed K = 1.0 for the remainder of the analysis. In fig. 4 we compare the measured values of $R(\sqrt{s};\bar{p},p)$ with the SLDM prediction, showing again a very good agreement.

V. Gluon Structure Function of the $\bar{p}$

Since the SLDM prediction of the x_F distribution using the DO set 1 structure functions for both the quarks and gluons agrees well with our data, any attempt to extract a gluon structure function through this model should lead to a result which is consistent with the DO set 1 gluon structure function over the kinematical range of the data. Here we investigate whether simpler forms for the gluon structure functions than that in DO set 1 can both reproduce the data and obey reasonable normalization constraints for the entire kinematical range. For this analysis, we have used as inputs the valence and sea quark structure functions given by DO set 1 and have parametrized the gluon structure functions of the beam antiproton and the target nucleons in two forms:

$$x\ G(x) = \beta\ (1 - x)^{\alpha} \qquad \text{(ref. 21)} \qquad (13)$$

and a more general form,

$$x\ G(x) = \beta\ (1 - x)^{\alpha}\ (1 + \gamma x) \qquad (14)$$

The parameters α, β, γ and the overall normalization N of the SLDM are determined from this fit. Although the parameters N and β have different physical origins, they are correlated since both contribute to the overall normalization.

The parameter β can be expressed as a function of the other parameters of eq. 13 and 14 using the momentum sum rule as an extra constraint. Our choice of the valence and sea quark structure functions implies that 52% of the nucleon momentum is carried by the quarks. Therefore, to conserve momentum the gluon structure function must satisfy:

$$\int_0^1 x\ G(x)\ dx = 0.48 \qquad (15)$$

Because we do not observe ψ production in our experiment ($\sqrt{s} = 15.3$ GeV/c^2 and $0.0 \leq x_F \leq 1.0$) over the entire x range of the integral (15) but only for $0.038 \leq x \leq 1.0$, we have assumed that the gluon structure function parametrization is valid for all regions of x in order to apply the constraint of eq. 15.

A second more dynamical way to use the momentum conservation constraint to determine β is to include in the fit the cross sections ratios $R(\sqrt{s};\bar{p},p)$ of Table 3 which are sensitive to the integral parton distributions.

Finally, rather than determining β apriori, we can constrain the overall normalization N and determine all the gluon structure function parameters. In this approach, the degree to which eq. 15 is satisfied by the fitted G(x) can be used as a criterion for deciding on the correctness of the extracted structure function. Tables 4a and 4b contain the results of the following fits:

E537$\bar{p}$-1 One parameter fit for α. The overall normalization was set to 0.188 and the parametrization of eq. 13 was used. β was determined as a

function of α using the momentum constraint of eq. 15, $\beta = 0.48\ (\alpha + 1)$.

E537$\bar{p}$-2 Two parameter fit of α and N. The parametrization of eq. 13 was used with the same β expression as in E537$\bar{p}$-1. No constraint was imposed on the overall normalization.

E537$\bar{p}$-3 Two parameter fit for α and β. The parametrization of eq. 13 was used with the overall normalization constrained to 0.188.

E537$\bar{p}$-4 Two parameter fit for α and N. We have included the SLDM prediction for the cross section ratios $R(\sqrt{s};\bar{p},p)$ with the DO set 1 quark structure functions and the gluon parametrization of eq. 13. The values R from Table 3 were used to express β as[17]

$\beta = 4.98 - 2.097\alpha + 0.323\alpha^2$

E537$\bar{p}$-5 Three parameter fit for α, β and γ using the gluon structure function parametrization of eq. 14 and constraining the overall normalization to N = 0.188.

TABLE 4a

Extracted gluon structure function parameters from the fits E537$\bar{p}$-1 through E537$\bar{p}$-5. Also shown is DO set 1 for comparison. (Note that the uncertainty due to the scaling of the cross sections to nb/nucleon is 3.1%).

FIT	χ^2/dof	N	α	β	γ
E537-$\bar{p}$1	1.8	0.188(fixed)	4.85±0.1	2.8 ±0.05	-
E537-$\bar{p}$2	1.0	0.22 ±0.03	6.00±0.9	3.37±0.4	-
E537-$\bar{p}$3	1.0	0.188(fixed)	6.32±0.3	4.47±0.4	-
E537-$\bar{p}$4	1.0	0.182±0.05	6.14±0.15	4.3 ±0.4	-
E537-$\bar{p}$5	1.0	0.188(fixed)	6.83±0.5	2.15±0.7	5.85±0.95
DO set 1	1.0	0.188±0.002	-	-	-

TABLE 4b

Fraction of momentum carried by gluons overall $0.0<x<1.0$, that for $0.038<x<1.0$ and the fraction ψ produced by gluon fusion for fits E537$\bar{p}$-1 through E537$\bar{p}$-5. The results for DO set 1 are shown for comparison.

E537	$\int_0^1 xG(x)dx$	$\int_{0.038}^1 xG(x)dx$	$\sigma_{gg}/\sigma_{gg}+\sigma_{q\bar{q}}$
E537-$\bar{p}$1	48%(fixed)	38%	45.5%±1%
E537-$\bar{p}$2	48%(fixed)	36%	39.0%±5%
E537-$\bar{p}$3	61%±6%	45%±4%	47.6%±3%
E537-$\bar{p}$4	63%±3%	47%±2%	50.0%±5%
E537-$\bar{p}$5	46%±3%	38%±2.5%	48.0%±3%
DO set 1	48%	38%	48%

Table 4b contains the integrated gluon momentum fraction for the entire x region ($0.0 < x < 1.0$) and for the region of sensitivity of the experiment ($0.038 < x < 1.0$). The fraction of ψ's produced through gluon fusion is also indicated. These quantities are calculated using the results of the fits from Table 4a. In contrast to the excellent fit of the SLDM with DO set 1 structure functions for both quarks and gluons, fit E537$\bar{p}$-1 has a poor χ^2 per degree of freedom. Since the DO set 1 quark structure functions reproduce our Drell-Yan data we conclude that the parametrization of eq. 13 is not adequate to describe the gluon structure function over the entire range in x. Keeping the same parametrization but increasing the number of free parameters in the fits E537$\bar{p}$-2 through E537$\bar{p}$-4, we find that the quality of fits are uniformly good and that the overall normalization N and the fraction of ψ's produced by gluon fusion do not change significantly with the fit. However, both the shape of the gluon structure function and the integrated gluon momentum fraction do change. The results of fit E537$\bar{p}$-5, with the more flexible parametrization, are in good agreement with the DO set 1 gluon structure functions, and give a reasonable value for the integrated gluon fraction. In fig. 5 we show the result of the fit E537$\bar{p}$-5 to our data.

The effects of heavy nuclear targets are most important at high x_F.[4] To check for the sensitivity to these effects, we have extracted the gluon structure function from the $\bar{p}$W data at $x_F \leq 0.5$ using the E537$\bar{p}$-1 through E537$\bar{p}$-5 parametrizations and constraints. The values of the parameters of the gluon distributions obtained using this limited x_F region are consistent within statistical errors with those obtained using the entire range of x_F.

Based on the arguments above, we choose the results of E537$\bar{p}$-5 as our best parametrization for the gluon structure function of the $\bar{p}$:

$$xG(x) = (2.15 * 0.7)\ [1 - x]^{(6.83 * 0.5)}\ [1 + (5.85 * 0.95)\ x]$$

VI. π^- gluon structure function

Following the method used to extract the gluon structure function of the antiproton in section V, we have determined the gluon structure function of the π^-. This is a more difficult undertaking since the π^- quark structure functions are not as well determined as the nucleon quark structure functions. In addition, since a larger percentage of ψ's produced in π^- collisions are in the high x_F region of the spectrum, we expect stronger nuclear targets effects.[4].

The fraction of ψ's produced via χ decay in π^- nucleon interactions has been measured by WA11[12] ($\sqrt{s}$ = 18.6 GeV) to be 0.305 (0.177 ± 0.035 ± 0.015 from χ^1 and 0.128 ± 0.023 ± 0.15 from χ^2 decays) and by experiment E673[16] ($\sqrt{s}$ = 18.9 GeV) to be 0.31 (0.2 ± 0.08 from χ^1 and 0.11 ± 0.06 from χ^2 decays).

For our extraction of the gluon structure functions of the π^-, we have used the WA11[12] measurements to set the fraction of ψ's coming from χ; the target nucleon DO set 1 gluon, valence and sea quark structure functions (they describe our $\bar{p}W$ data very well); the NA3 determination of the sea quark pion structure function $0.238\ (1 - x)^{8.7}$ which predicts that 15% of the total momentum is carried by the sea quarks;[8] and the π^- valence quarks the structure functions determined from our own measurements of Drell-Yan production of high mass muon pairs;[6,22,23]

The parametrization of ref. 6b of the valence quark structure function of the π^-:

$$xV(x) = Ax^a\ (1 - x)^b \qquad (17)$$

has been scaled to $Q^2 = M_\psi^2$ using the method of Altarelli-Parisi[24] to obtain the values of A, a, and b given in Table 5. Also shown in the table is the NA3 valence quark structure function[8] for comparison. The different E537π^- fits correspond to different normalization constraints to our Drell-Yan data.[6,23]

TABLE 5

Valence quark structure function parameters of refs. 6, 22 and 23 evolved to $Q^2 = M_\psi^2$ and of ref. 8 used in extracting the gluon structure function of the π^-. The fit names are different from the quoted references as they have been scaled to a different value of Q^2.

Set	A	a	b	$\int_0^1 xVdx$
E537π^--1	0.82	0.51	1.16	38%
E537π^--2	0.681	0.454	1.125	35%
E537π^--3	0.8164	0.51	1.166	38%
E537π^--4	0.76	0.49	1.15	37%
NA3 (ref. 8)	0.52	0.40	0.78	56%

With these various choices for the quark structure functions, we parametrize the gluon distribution of the π^- as $xG(x) = \beta\ (1\text{-}x)^{\alpha}$. We have fitted both our W and Be data using the quark distributions of Table 5 as input to the SLDM, leaving the overall normalization and the exponent α free to vary. The results for W and Be targets are shown in Table 6, along with the calculated fraction of the ψ produced via gluon fusion in π^-W and π^-Be interactions.

TABLE 6

The parameters of the π^- gluon structure function obtained by fitting with different input valence quark distributions, V(x), for the W and Be data. The calculated fractions of ψ produced via gluon fusion is also shown. Note that the error due to the scaling of the cross section to nb/nucleon is an additional 3.1%.

V(x)	$\beta/\alpha+1$ (fixed)	α(W)	α(Be)	N(W)	N(Be)	$\sigma_{gg}/\sigma_{\pi^-}$ (W)	$\sigma_{gg}/\sigma_{\pi^-}$ (Be)
E537π^--1	49%	2.0 ±0.06	1.3±0.2	0.191±0.002	0.17 ±0.004	70.4±2%	73±7%
E537π^--2	50%	1.98±0.06	1.2±0.2	0.187±0.002	0.17 ±0.004	74 ±2%	76±8%
E537π^--3	47%	2.0 ±0.06	1.3±0.2	0.192±0.002	0.173±0.004	71 ±2%	74±7%
E537π^--4	48%	1.98±0.06	1.2±0.2	0.190±0.002	0.17 ±0.004	72 ±2%	75±8%
NA3(ref.8)	49%	2.03±0.06	1.3±0.2	0.193±0.002	0.17 ±0.004	73 ±3%	75±7%

The resulting value of the overall normalization constant is in agreement with that obtained using the SLDM with our $\bar{p}$ data. As shown in Table 6, the extracted gluon structure functions are not sensitive to the choice of the quark structure function set, but they depend strongly on the particular target nucleus used. In fig. 6 we present our data for W and the prediction of the SLDM model using the E537π^--2 pion valence quark structure function. Similarly, in fig. 7 we compare our Be data to the SLDM predictions with the E537π^--2 quark structure functions. The solid line represents the prediction with the best fit for the gluon structure function extracted from the Be data. The prediction utilizing the gluon structure function based on the best fit to the W data is included in fig. 7 to show the strength of the A dependence.

As in the case of determining the $\bar{p}$ gluon structure function we use the ratios of the ψ production cross sections to check the validity of the fits. The ratios of the production cross sections for $pN \rightarrow \psi + X$ to $\pi^- N \rightarrow \psi + X$:

$$R(\sqrt{s};\ p,\pi^-) = \frac{\sigma(pN \rightarrow \psi + x)}{\sigma(\pi^- N \rightarrow \psi + x)}$$

are sensitive only to the integral of the parton distribution functions. In Table 7 we summarize the measured ratios as function of beam energy from several experiments.

TABLE 7

Cross section ratios for ψ production by p and π^- beams on nuclear targets measured at different energies. To obtain the ratio for this experiment (E537) we have used the Lyons[20] cross section for protons.

Experiment	Beam Momentum (GeV/c)	$\sqrt{s}$ (GeV/c2)	$\sigma_p/\sigma_{\pi^-}=R(\sqrt{s};p,\pi^-)$
Ω (ref. 19)	39.5	8.6	0.17 ± 0.02
E-537	125.0	15.3	0.45 ± 0.05
NA3 (ref. 8)	150.0	16.8	0.42 ± 0.04
NA3 (ref. 8)	200.0	19.4	0.53 ± 0.05

Using the SLDM prediction for the $R(\sqrt{s})$ with the nucleon quark distributions mentioned above, the E-537-2 quark structure function for the valence quarks of the π^-, and the values of Table 7, we have determined the dependence of β as a function of α to be:[17]

$$\beta = 0.562 + 0.3165 \quad \alpha + 0.139 \quad \alpha^2 \tag{19}$$

We have fitted both our Be and W data using eq. (19), replacing β / (α + 1), as the constraint for the gluon normalization. The exponent α and the overall normalization N were left free to vary. The results for both targets are presented in Table 8.

TABLE 8

Fit for the parameters of the gluon structure function, $xG(x) = N\ (1 - x)^{\alpha}$, of the π^- with the E537π^--2 quark structure function using eq. 19 as momentum constraint.

Target	α	N	$\int_0^1 xG(x)dx$	$\int_{0.2}^1 xG(x)dx$	$\sigma_{gg}/(\sigma_{gg}+\sigma_{q\bar{q}})$
W	1.96±0.05	0.17±0.01	58±5%	30±3%	75±2%
Be	1.3 ±0.3	0.16±0.04	52±8%	31±5%	72±7%

The value of a obtained is consistent with the ones from the previous fits in Table 6. We have not attempted a more general parametrization of the gluon structure function (as in the $\bar{p}$ case, eq. 14) because of distortions by nuclear effects of our high statistic W data.

The gluon structure functions extracted from the Be and the W data have been used in the SLDM formalism to predict the ratio of the total cross section σ_p/σ_{π^-} as a function of beam momentum. This prediction is compared in fig. 8, to data from Table 7. The momentum dependence of the ratio σ_p/σ_{π^-} is described satisfactorily by both sets of structure functions.

For comparison, experiment NA3[8] has extracted the gluon structure function of the π from the "hard component" of ψ production in π^- Pt interactions using an analysis with significantly different assumptions about the production model for the ψ's:

$$xG(x) \sim (1 - x)^{2.38 \pm 0.06 \pm 0.1} \qquad (20)$$

WA11[12] using a Be target has extracted a gluon structure function:

$$xG(x) \sim (1 - x)^{1.9 \pm 0.3} \qquad (21)$$

Our best estimation of the π^- gluon structure function is:

$$xG(x) = (1.49 \pm 0.03)\ [1 - x]^{(1.98 \pm 0.06)} \quad \text{from the } \pi^-\text{W data}$$

and

$$xG(x) = (1.10 \pm 0.10)\ [1 - x]^{(1.20 \pm 0.2)} \quad \text{from the } \pi^-\text{Be data.}$$

VII. Transverse momentum of the ψ

Since the SLDM model contains only the intrinsic transverse momentum of the $c\bar{c}$ pairs, it does not completely describe the p_t spectrum of the ψ's. In fact, a comprehensive model for the transverse momentum of ψ production does not presently exist. Furthermore, the smearing of the p_t distribution of the ψ's caused by the indirect ψ production from $\chi \rightarrow \psi + \gamma$ decays is a complication in any attempt to extract information from the p_t distribution. Therefore, we have not attempted a detailed analysis of our measured p_t spectra. In figs. 9(a) and 9(b) we present the $d\sigma/dp_t^2$ spectra for $\bar{p}W$ and π^-W. The experimental data is well described by the empirical form

$$(1 + p_t^2/a^2)^{\beta} \qquad (22)$$

with $a = 2.79 \pm 0.2$, $\beta = -8.03 \pm 0.96$ for $\bar{p}W$ data and $a = 2.67 \pm 0.12$ $\beta = -6.87 \pm 0.5$ for π^-W data.

In figs. 10(a) and 10(b) we show the variation of the $\langle p_t \rangle$ as a function of x_F. In ref. 6, we showed that nuclear effects distort the shape of the p_t distribution independently of the x_F region examined. Therefore, the systematic decrease of the mean p_t vs. x_F appears not to be caused by heavy nucleus effects.

V. Angular distributions

Finally, we have studied the angular distributions of the ψ's to gain additional information about the ψ production mechanism.[25] We show the Gottfried-Jackson[26] frame angular distributions in θ is the angle of positive muon with respect to the beam in the rest frame of the ψ. Figs. 11(a) and 11(b) show that the angular distributions are essentially flat. Fitting the angular distributions to the form:

$$d\sigma/d\cos\theta \quad \alpha \quad 1 + \lambda \cos^2\theta \qquad (23)$$

we obtain λ = -0.115 ± 0.061 for $\bar{p}$'s and λ = 0.028 ± 0.004 for π^-'s. Similarly, the azimuthal angle ϕ distribution is flat as shown in figs. 12(a) and 12(b). The isotropic behavior of the data is independent of the x_F and p_t regions in both $\bar{p}$ and π^- interactions as shown in figs. 13 and 14.

We have also studied the A dependence of the ψ production cross sections as a function of cosθ and ϕ by forming the ratios:

$$r_1(\cos\theta;W,Be) = \frac{\frac{1}{A_W}\left[\frac{d\sigma}{d\cos\theta}\right]_W}{\frac{1}{A_{Be}}\left[\frac{d\sigma}{d\cos\theta}\right]_{Be}} \qquad (24)$$

and

$$r_2(\phi;W,Be) = \frac{\frac{1}{A_W}\left[\frac{d\sigma}{d\phi}\right]_W}{\frac{1}{A_{Be}}\left[\frac{d\sigma}{d\phi}\right]_{Be}} \qquad (25)$$

These ratios are shown in figs. 15 and 16. Both ratios r_1 and r_2 are flat as a function of cosθ and ϕ for both beam types, and their average values are consistent with the overall suppression of ψ production in the heavy target (0.73 ± 0.04 for $\bar{p}$ beam and 0.70 ± 0.02 for π^- beam).

VI. Conclusions

We have studied ψ hadronic production in $\bar{p}$N and π^-N interactions at 125 GeV/c. We have measured the total cross section for the production of ψ and ψ', the differential cross section $d\sigma/dx_F$ for both $\bar{p}$ and π^- beams with W and Be targets. We have determined the gluon structure functions of the $\bar{p}$'s and π^-'s by fitting the x_F distributions

using different parametrizations and constraints. For the antiproton we find a parametrization which is in good agreement with our experimental data and the Duke and Owens (set 1) structure functions

$$xG(x)_{\bar{p}} = (2.15 \pm 0.7)\ [1 - x]^{(6.83 \pm 0.5)}\ \ [1 + (5.85 \pm 0.95)x]$$

Nuclear target effects distort significantly the shape of the x_F distributions for our π^- data and as a result we give gluon structure functions separately for π^-W and π^-Be data:

$$xG(x)_{\pi^-} = (1.49 \pm 0.03)\ [1 - x]^{(1.98 \pm 0.06)} \qquad \text{from } \pi^-\text{W production of } \psi\text{'s}$$

$$xG(x)_{\pi^-} = (1.10 \pm 0.10)\ [1 - x]^{(1.20 \pm 0.2)} \qquad \text{from } \pi^-\text{Be production.}$$

We have also measured the transverse momentum and decay angular distributions of the ψ's. Isotropic angular distributions are observed. No strong correlation between x_F and $\langle p_t \rangle$ is found.

VII. References

1. See for example: R. Baier & R. Rückl, *Z. Phys. C*, 19, 251 (1983).
2. J.J. Aubert et al., *Nuc. Phys.* B293, 740 (1987).
3. J.J. Aubert et al., *Nuc. Phys.* B272, 158 (1986).
4. S. Katsanevas et al., *Phys. Rev. Lett.* 60, 2121 (1988).
5. E. Anassontzis et al., *Nucl. Inst. Meth.* 242A, 215 (1986).
6. a)E. Anassontzis et al., *Phys. Rev. Lett.* 54, 2572 (1985).
   b)E. Anassontzis et al., *Phys. Rev. D* 38, 1377 (1988).
7. H. Areti et al., *Nucl. Inst. Meth.* 212, 135 (1983).
8. J. Badier et al., *Z. Phys. C* 20, 101 (1983).
9. J.P. Blaizot and J. Ollitrault, *Phys. Lett.* 217B, 392 (1989).
10. G. Baglin et al., *Phys. Lett.* 220B, 471 (1989).
11. Particle Properties Data, *Phys. Lett.* 204B, (1988).
12. Y. Lemoigne et al., *Phys. Lett.* 113B, 509 (1982).
    J.G. McEwen et al., *Phys. Lett.* 121B, 198 (1983).
13. C.E. Carlson and R. Suaya, *Phys. Rev. D* 18, 760 (1978).
    L. Clavelli et al., *Phys. Rev. D* 31, 482 (1985).
    L. Clavelli et al., *Phys. Rev. D* 32, 612 (1985).
    See also refs. 1 and 18.
14. M. Glück et al., *Phys. Rev. D* 17, 2324 (1978).
    M. Glück and E. Reya, *Phys. Lett.* 79B, 453 (1978).
    V. Barger et al., *Z. Phys. C* 6, 169 (1980).
    V. Barger et al., *Phys. Lett.* 91B, 253 (1980).
    P. Chiappetta and P. Mery, *Phys. Rev. D* 32, 2337 (1985).
15. C. Kourkoumelis et al., *Phys. Lett.* 81B, 405 (1979).
16. D.A. Bauer et al., *Phys. Rev. Lett.* 54, 753 (1985).
17. G. Voulgaris, Ph.D. Thesis, University of Athens, 1984.

S. Tzamarias, Ph.D. Thesis, University of Athens, 1986.

18. D.W. Duke and J.F. Owens, *Phys. Rev. D* 30, 49 (1984).

19. M. J. Corden et al., *Phys. Lett.* 96B, 411 (1980).

20. L. Lyons, *Prog. Part. Nucl. Phys.* 7, 169 (1981).

21. A.J. Buras et al., *Nuc. Phys.* 131B, 308 (1977).

A.J. Buras and K.J.F. Gaemers, *Nucl. Phys.* 132B, 249 (1978).

22. S. Katsanevas, Ph.D. Thesis, University of Athens 1982.

23. W. Shappert, Ph.D. Thesis, McGill University 1984.

24. G. Altarelli and G. Parisi, *Nucl. Phys.* 126B, 298 (1977).

25. B. L. Ioffe, *Phys. Rev. Lett.* 39, 1589 (1977).

J. Cleymans et al., *Phys. Lett.* 106B, 143 (1981).

J. H. Kühn, *Phys. Lett.* 89B, 385 (1980).

26. K. Gottfried & J.D. Jackson, *Nuov. Cim.* 33, 309 (1964).

VIII. Figure Captions

Figure 1. The E537 spectrometer.

Figure 2. (a) $\mu^+\mu^-$ invariant mass for π^-W interactions. (b) $\mu^+\mu^-$ invariant mass for $\bar{p}$W interactions.

Figure 3. $d\sigma/dx_F$ spectra for this experiment's $\bar{p}$W data. The solid line is the SLDM prediction using DO set 1 structure functions and keeping the overall normalization as a free parameter. The dash line represents the $q\bar{q} \rightarrow \psi$ contribution while the dotted-dashed line the $gg \rightarrow \psi$ contribution.

Figure 4. Comparison of the ratios of inclusive ψ production cross sections from $\bar{p}$N and pN interactions (Table 3) with the prediction of the SLDM using DO set 1 structure functions.

Figure 5. $d\sigma/dx_F$ distribution for this experiment's $\bar{p}$W data. The solid line represents the best fit of the parametrization of the gluon structure function $xG(x)=\beta(1-x)^{\alpha}(1+\gamma x)$. The dashed line and the dotted-dashed line are the $q\bar{q}$ and gg contributions respectively.

Figure 6. Best fit using the E537π^--2 quark structure functions for this experiment's π^-W $d\sigma/dx_F$ data (solid line). The dashed and the dotted-dashed line are the gg and the $q\bar{q}$ contributions respectively.

Figure 7. $d\sigma/dx_F$ for this experiment's π^-Be data. The solid line is the best fit using E537π^--2 quark structure functions. The band shows the range of predictions

from the SLDM varying the π^- gluon structure function parameters extracted from the W data by $\pm$ one standard deviation from the best fit. The effect of the heavier nuclear target is clear.

Figure 8. Comparison of the ratios of the inclusive ψ production cross sections from p and π^- of Table 7 with the predictions of the SLDM using the E537π^--2 quark structure functions and the gluon structure function extracted from this experiment's Be data (solid line) and W data (dashed line).

Figure 9. $d\sigma/dp_t^2$ vs. p_t^2 for this experiment's (a) $\bar{p}W$ and (b) π^-W data. The solid lines are empirical fits.

Figure 10. $<p_t>$ vs. x_F for this experiment's (a) $\bar{p}W$ and (b) π^-W data.

Figure 11. $\cos\theta$ distributions for this experiment's (a) $\bar{p}W$ and (b)π^-W data.

Figure 12. ϕ distribution of this experiment's (a) $\bar{p}W$ and (b) π^-W data.

Figure 13. λ as a function of p_t, integrated over all x_F, for this experiment's (a) $\bar{p}W$ and (b) π^-W data.

Figure 14. λ as a function of x_F, integrated over all p_t, for this experiment's (a) $\bar{p}W$ and (b) π^-W data.

Figure 15. Ratio of differential cross sections r_1 (see text) as a function of $\cos\theta$ for this experiment's (a) $\bar{p}W$ and (b) π^-W data.

Figure 16. Ratio of differential cross sections r_2 (see text) as a function of ϕ for this experiment's(a) $\bar{p}W$ and (b) π^-W data.

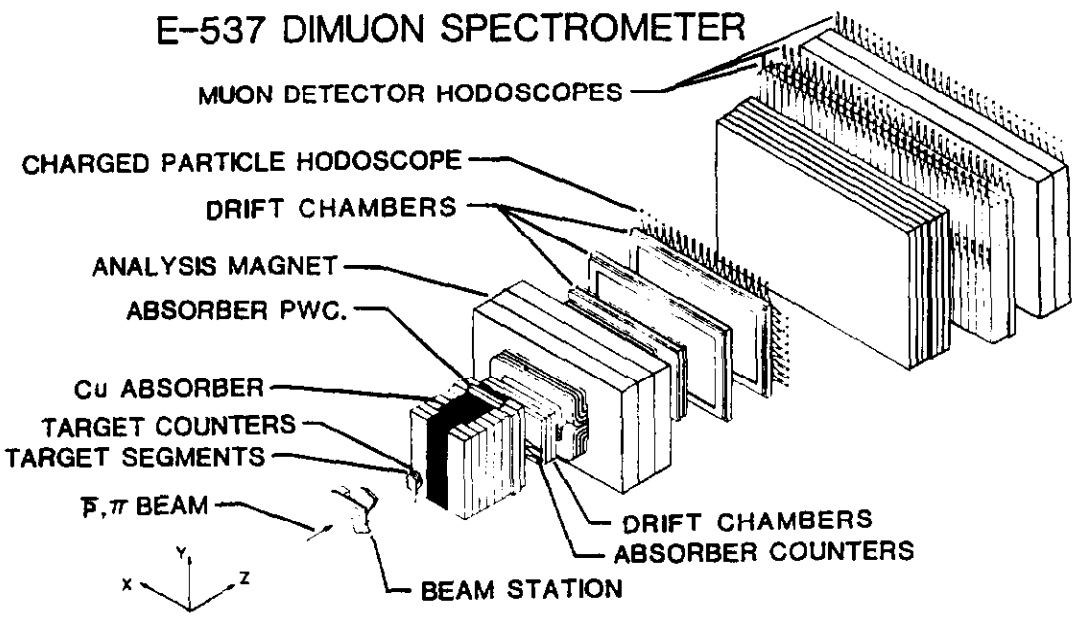

Figure 1. The E537 spectrometer.

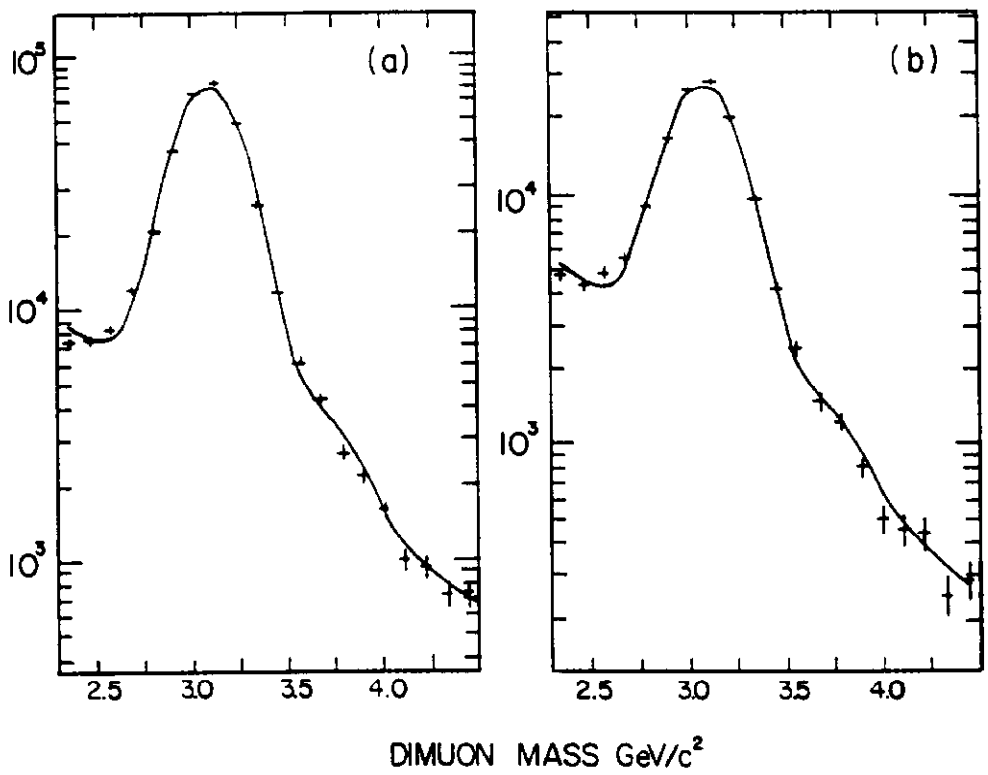

Figure 2. (a) $\mu^+\mu^-$ invariant mass for π^-W interactions. (b) $\mu^+\mu^-$ invariant mass for $\bar{p}$W interactions.

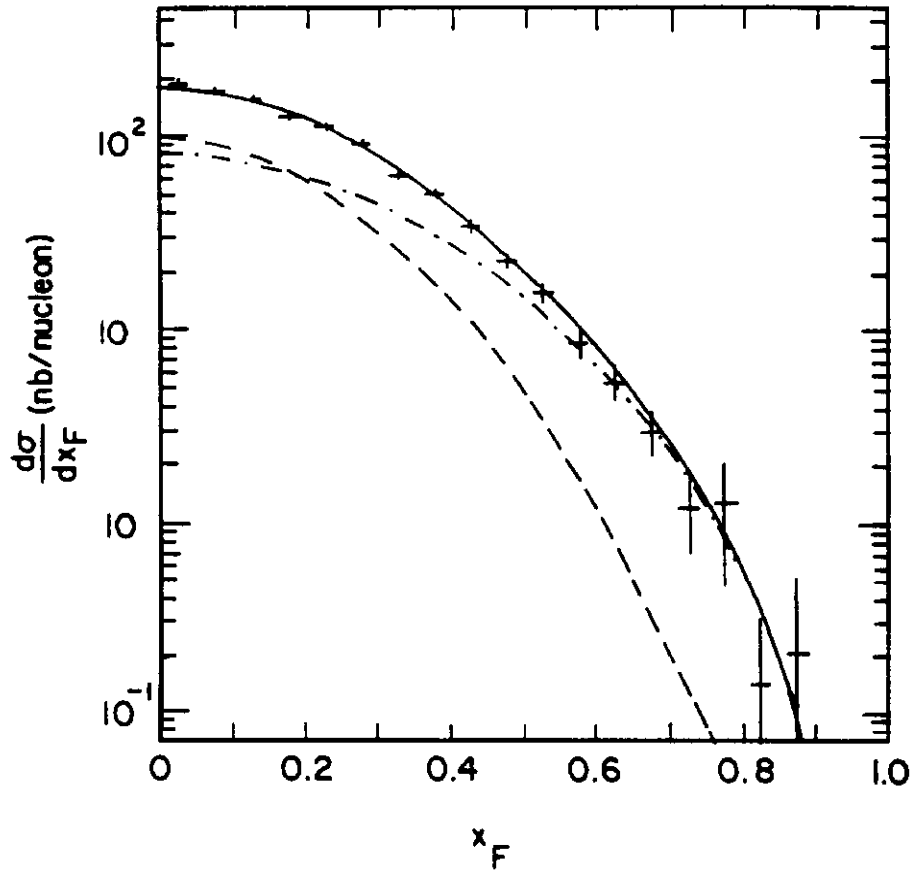

Figure 3. $d\sigma/dx_F$ spectra for this experiment's $\bar{p}W$ data. The solid line is the SLDM prediction using DO set 1 structure functions and keeping the overall normalization as a free parameter. The dash line represents the $q\bar{q} \rightarrow \psi$ contribution while the dotted-dashed line the $gg \rightarrow \psi$ contribution.

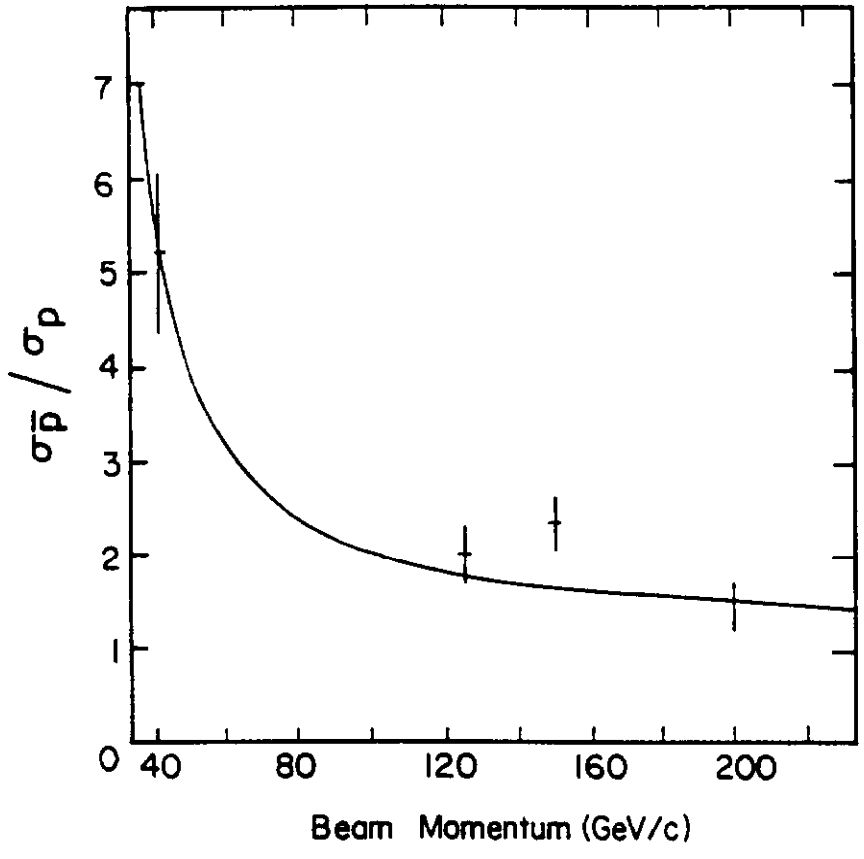

Figure 4. Comparison of the ratios of inclusive ψ production cross sections from $\bar{p}N$ and pN interactions (Table 3) with the prediction of the SLDM using DO set 1 structure functions.

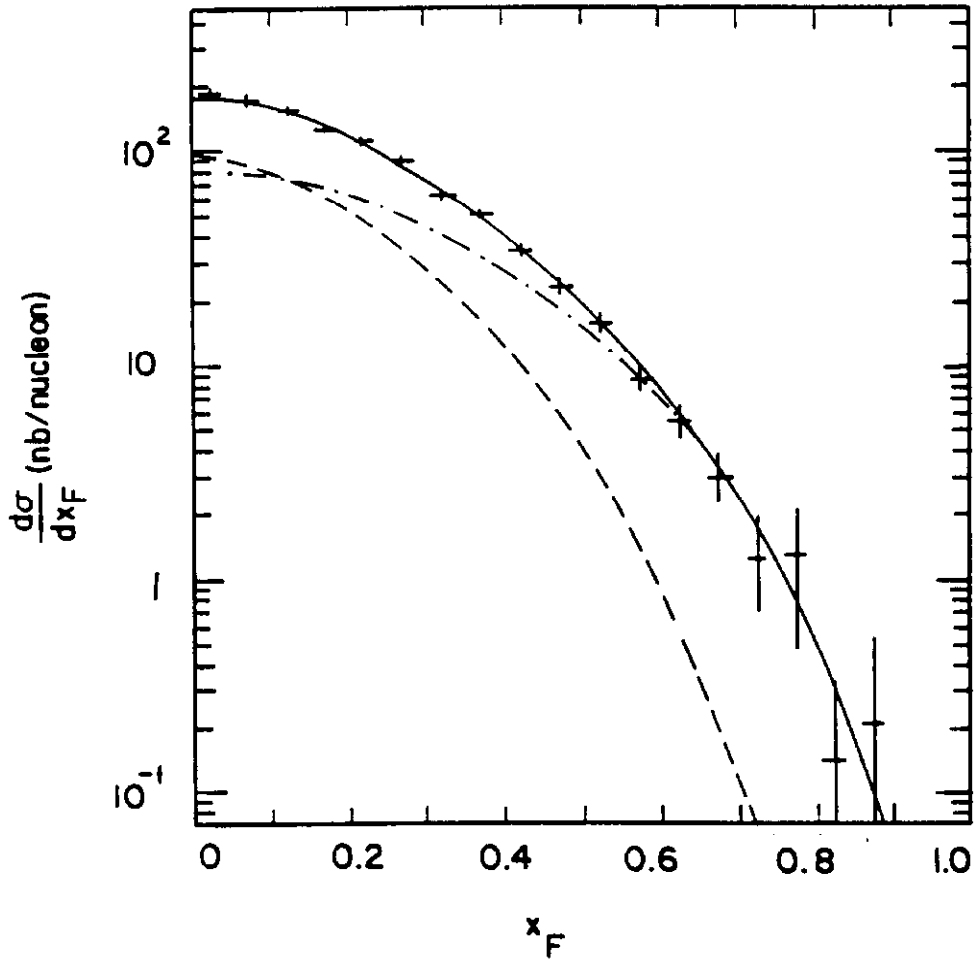

Figure 5. $d\sigma/dx_F$ distribution for this experiment's $\bar{p}W$ data. The solid line represents the best fit of the parametrization of the gluon structure function $xG(x)=\beta(1-x)^{\alpha}(1+\gamma x)$. The dashed line and the dotted-dashed line are the $q\bar{q}$ and gg contributions respectively.

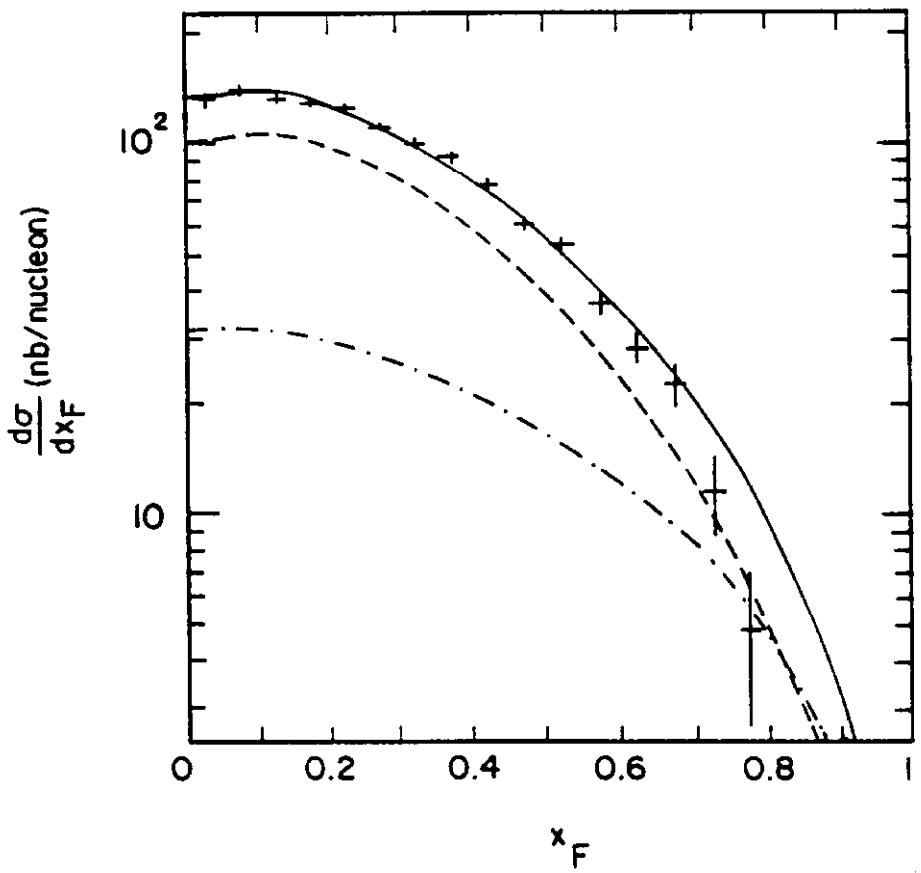

Figure 6. Best fit using the E537π^--2 quark structure functions for this experiment's π^-W $d\sigma/dx_F$ data (solid line). The dashed and the dotted-dashed line are the gg and the $q\bar{q}$ contributions respectively.

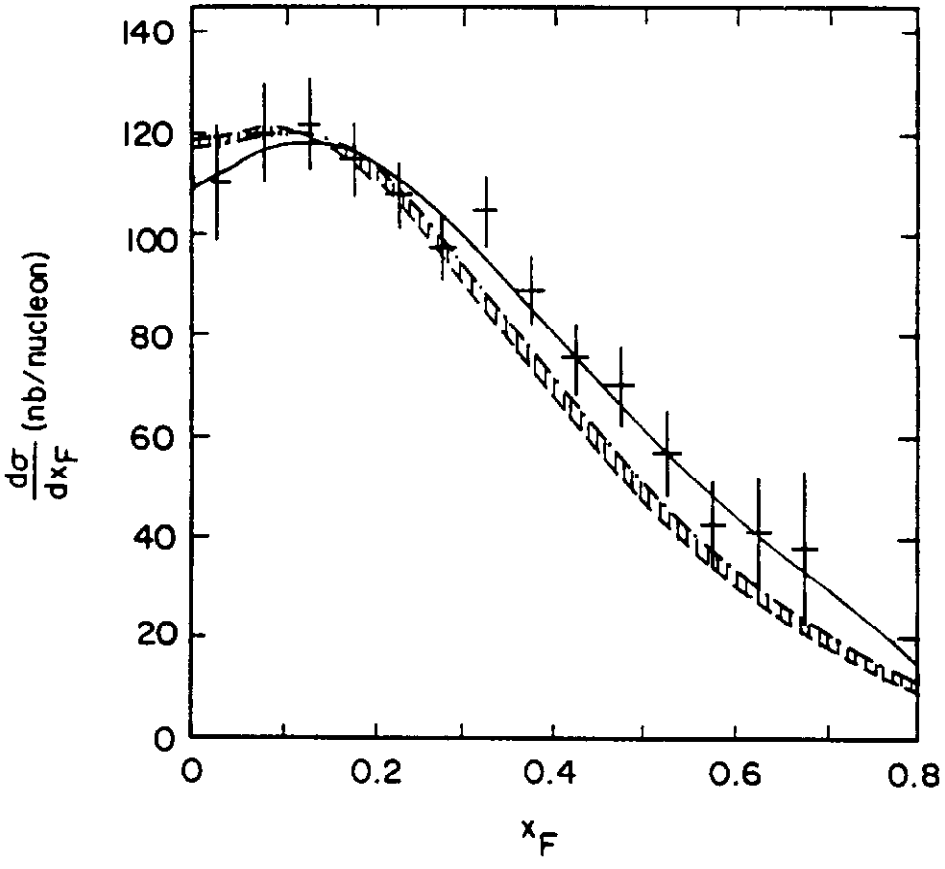

Figure 7. $d\sigma/dx_F$ for this experiment's π^-Be data. The solid line is the best fit using E537π^--2 quark structure functions. The band shows the range of predictions from the SLDM varying the π^- gluon structure function parameters extracted from the W data by ± one standard deviation from the best fit. The effect of the heavier target is clear.

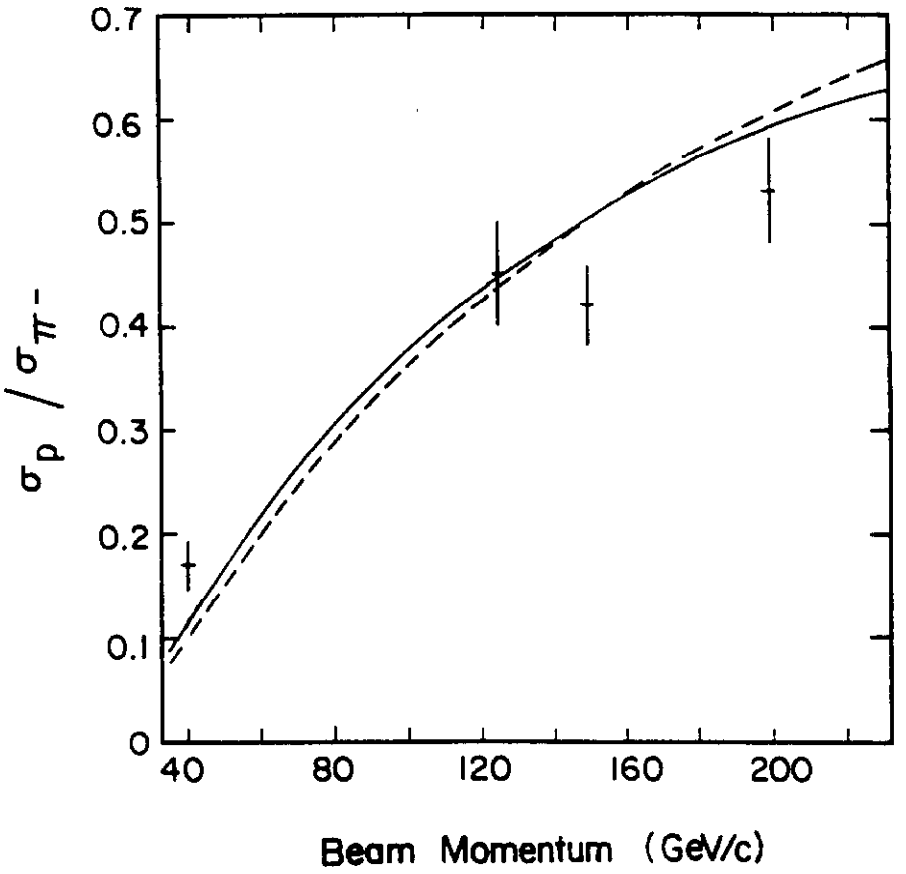

Figure 8. Ratios of the inclusive ψ production cross sections from p and π^- (Table 7) and the predictions of the SLDM using the E537π^--2 quark structure functions and the gluon structure function extracted from this experiment's Be data (solid line) and W data (dashed line).

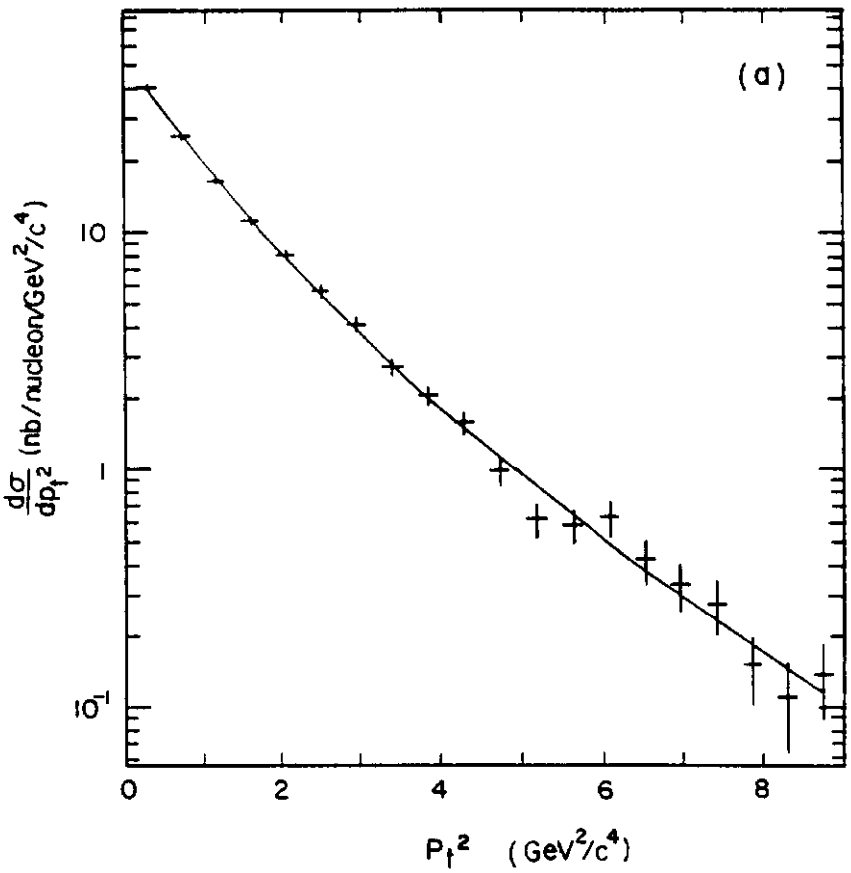

Figure 9a. $d\sigma/dp_t^2$ vs. p_t^2 for this experiment's $\bar{p}W$. The solid line is an empirical fit.

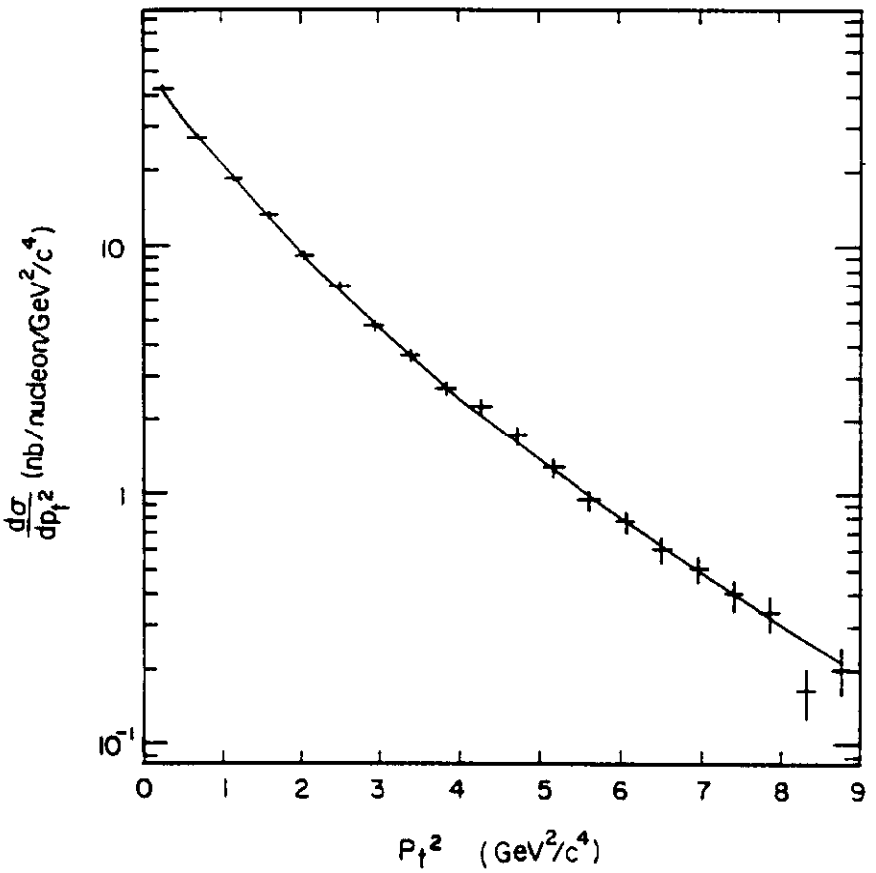

Figure 9b. $d\sigma/dp_t^2$ vs. p_t^2 for this experiment's π^-W data. The solid line is an empirical fit.

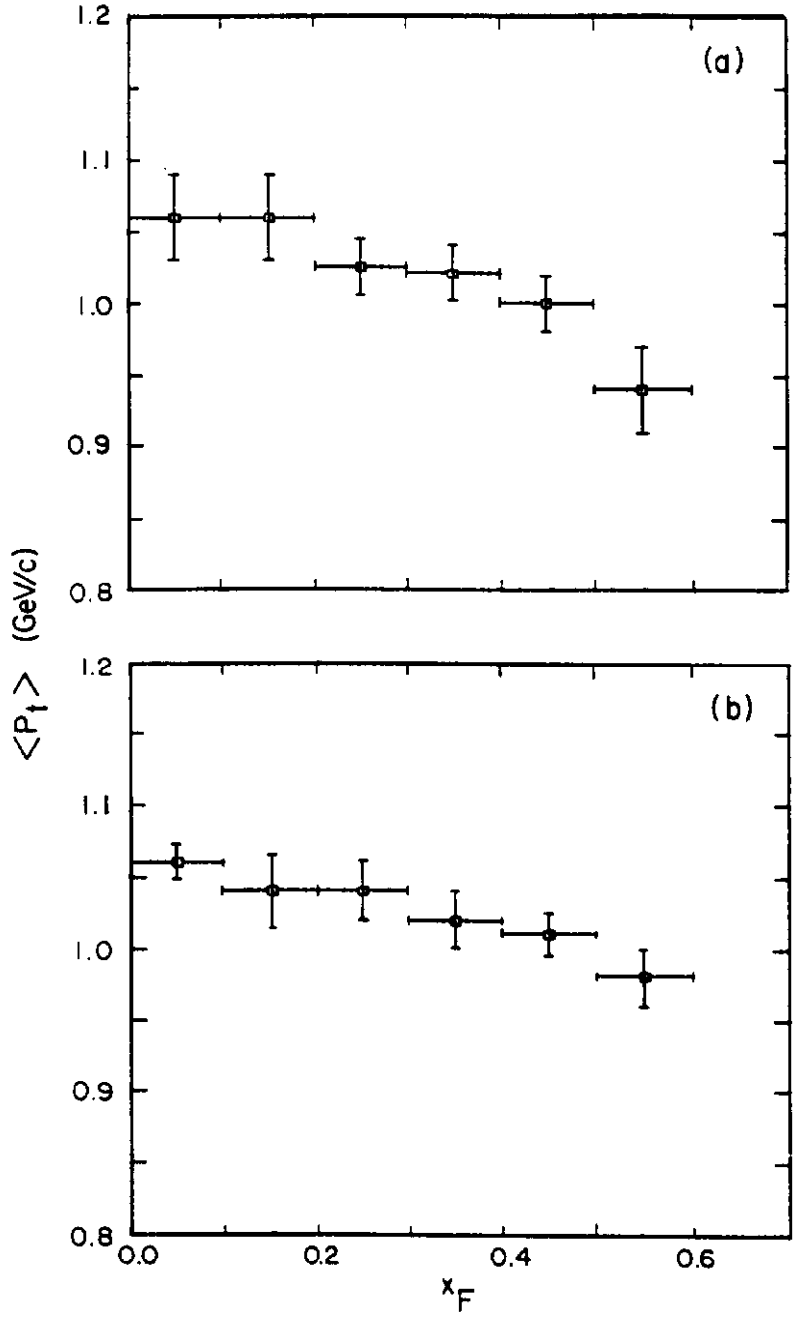

Figure 10. $<p_t>$ vs. x_F for this experiment's (a) $\bar{p}W$ data and (b) the $\pi^- W$ data.

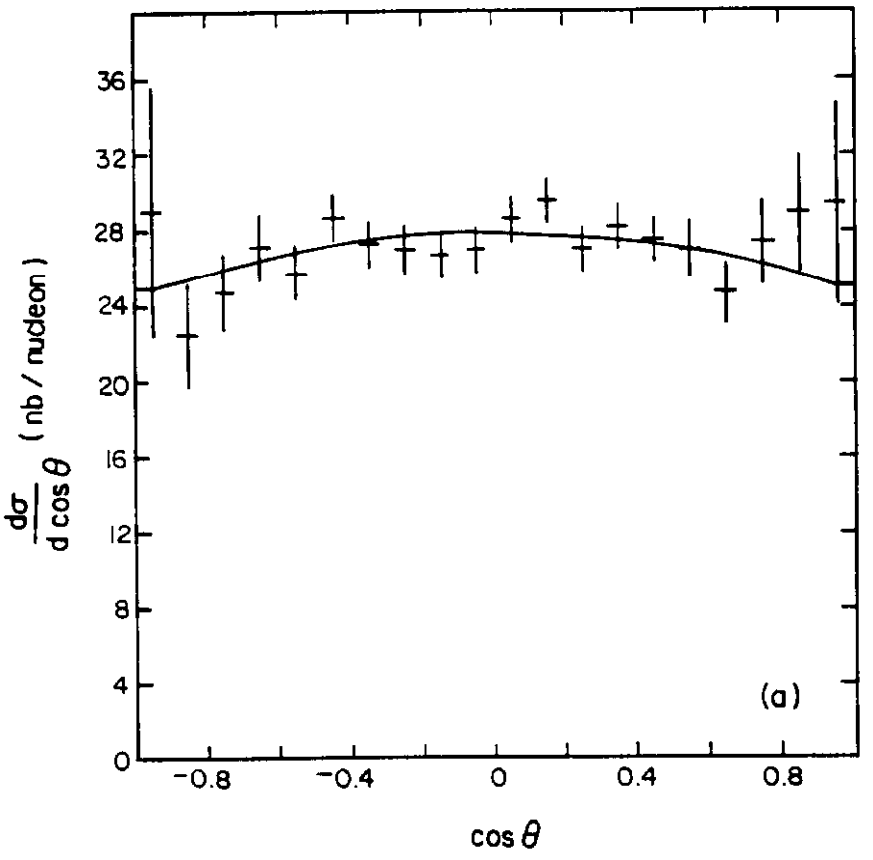

Figure 11a. $\cos\theta$ distributions for this experiment's $\bar{p}W$ data.

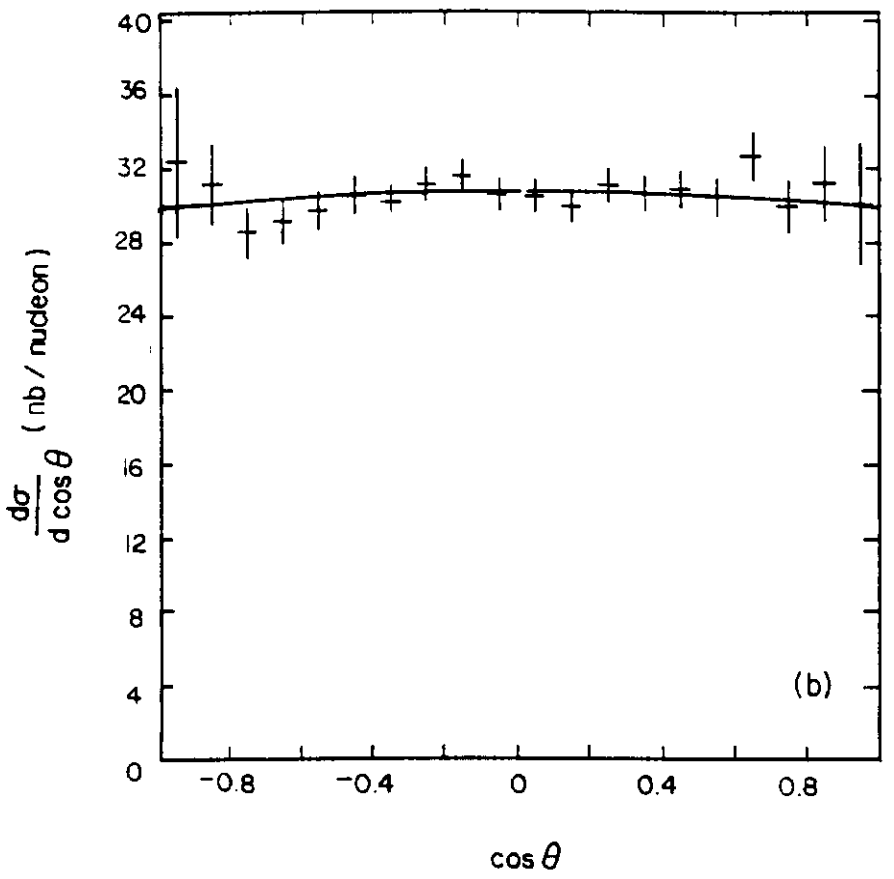

Figure 11b. $\cos\theta$ distributions for this experiment's π^-W data.

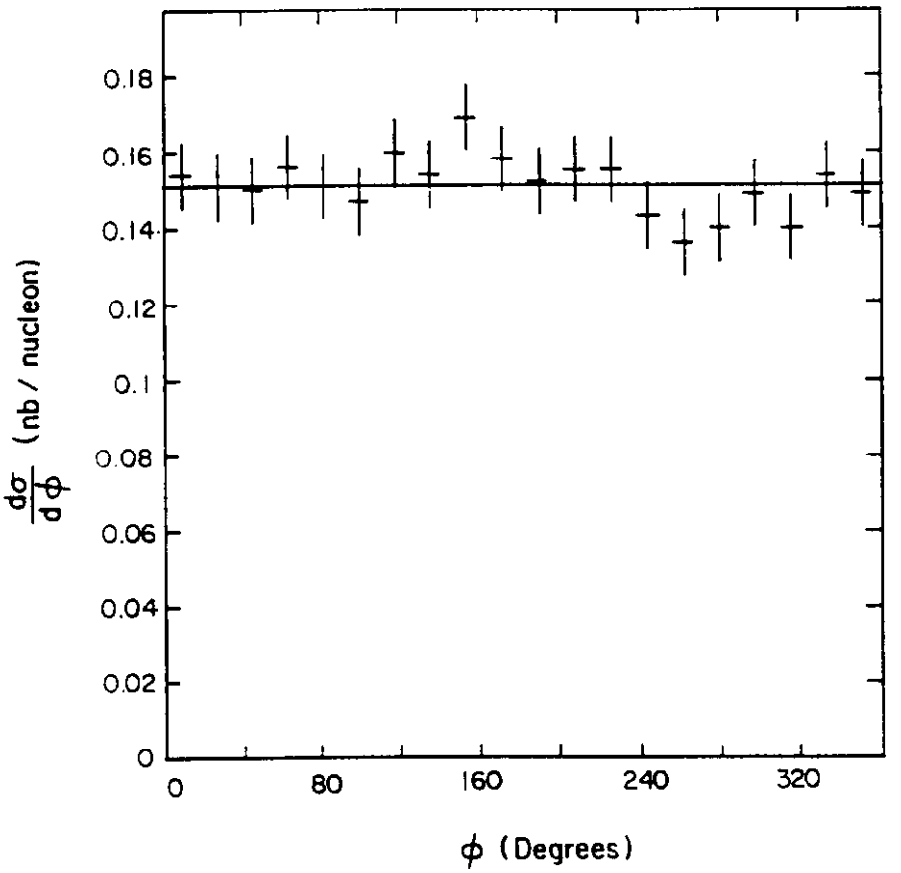

Figure 12a. ϕ distribution for this experiment's $\bar{p}W$ data.

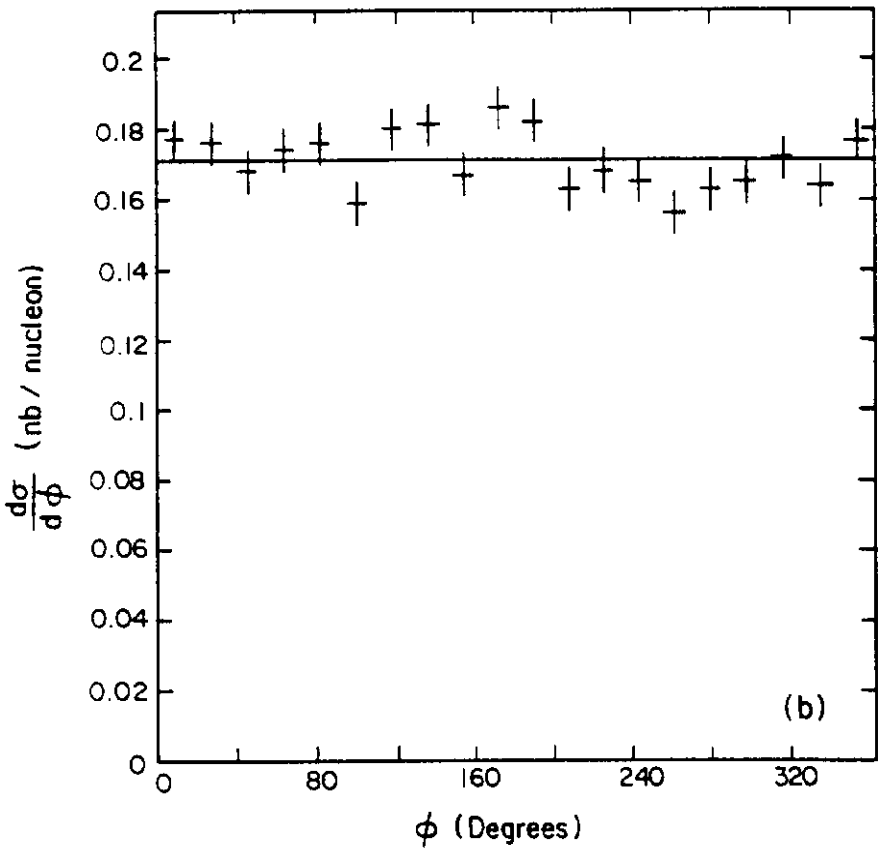

Figure 12b. ϕ distribution for this experiment's π^-W data.

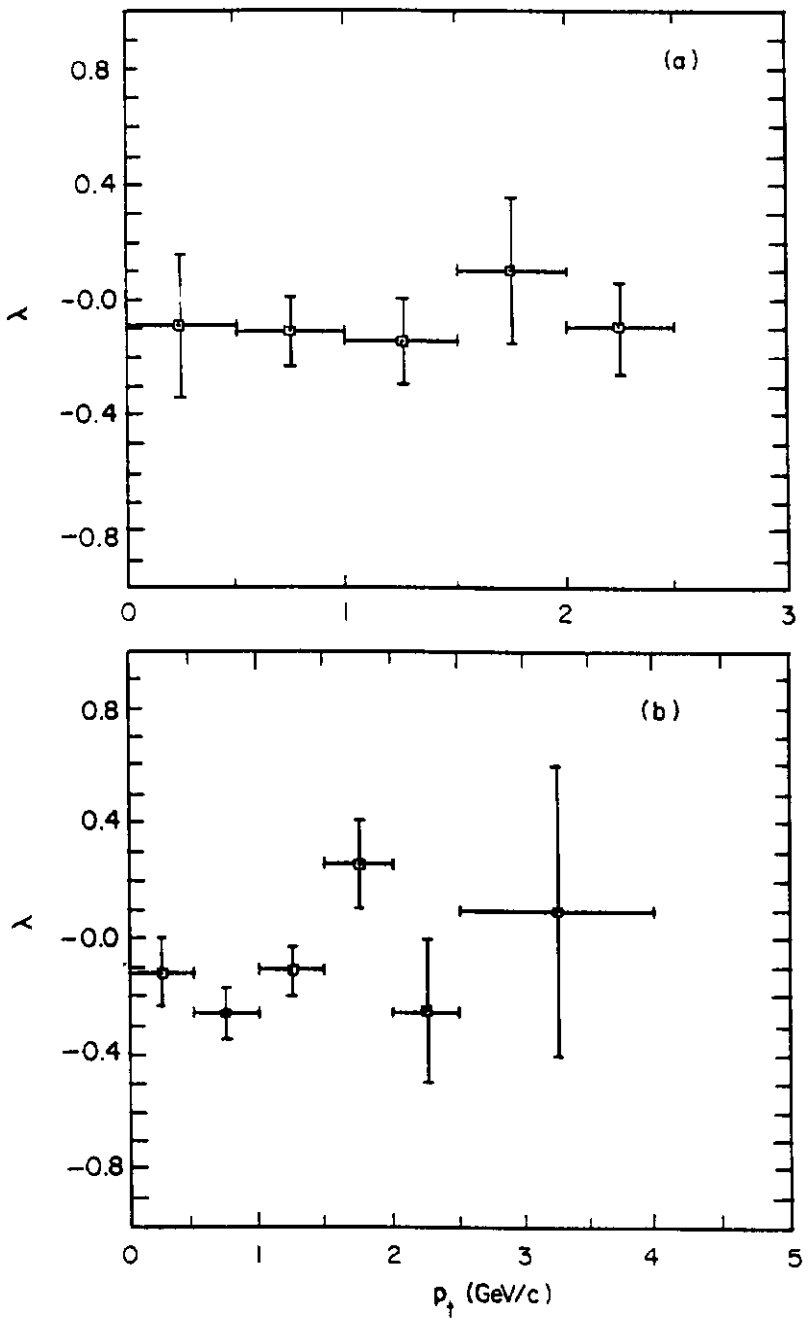

Figure 13. λ as a function of p_t, integrated over all x_F, for this experiment's (a) $\bar{p}W$ data and (b) $\pi^- W$ data.

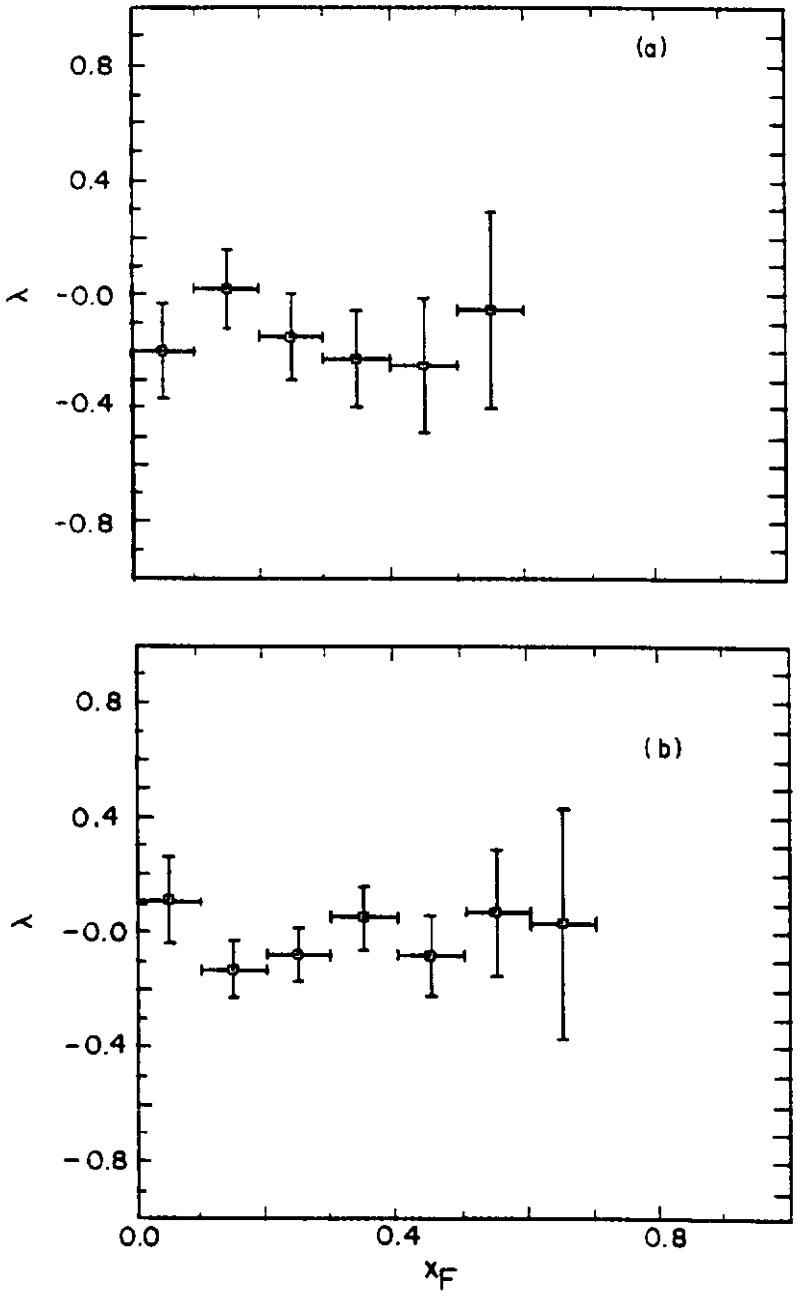

Figure 14. λ as a function of x_F, integrated over all p_t, for this experiment's (a) $\bar{p}W$ data and (b) $\pi^- W$ data.

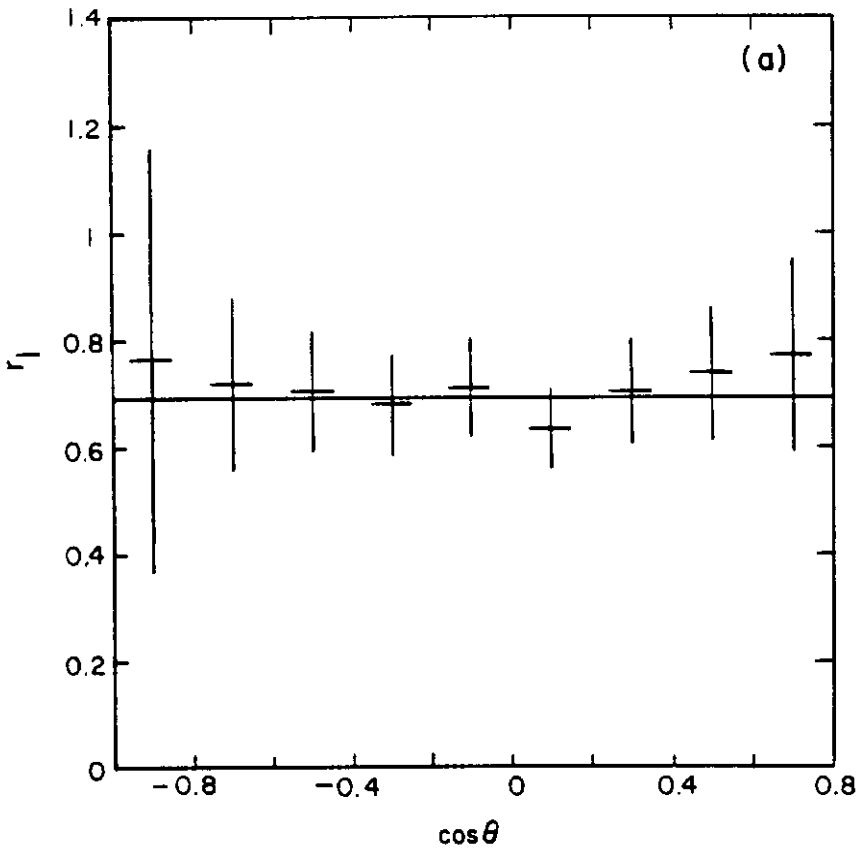

Figure 15a. Ratio of differential cross sections r_1 (see text) as a function of $\cos\theta$ for this experiment's $\bar{p}W$ data.

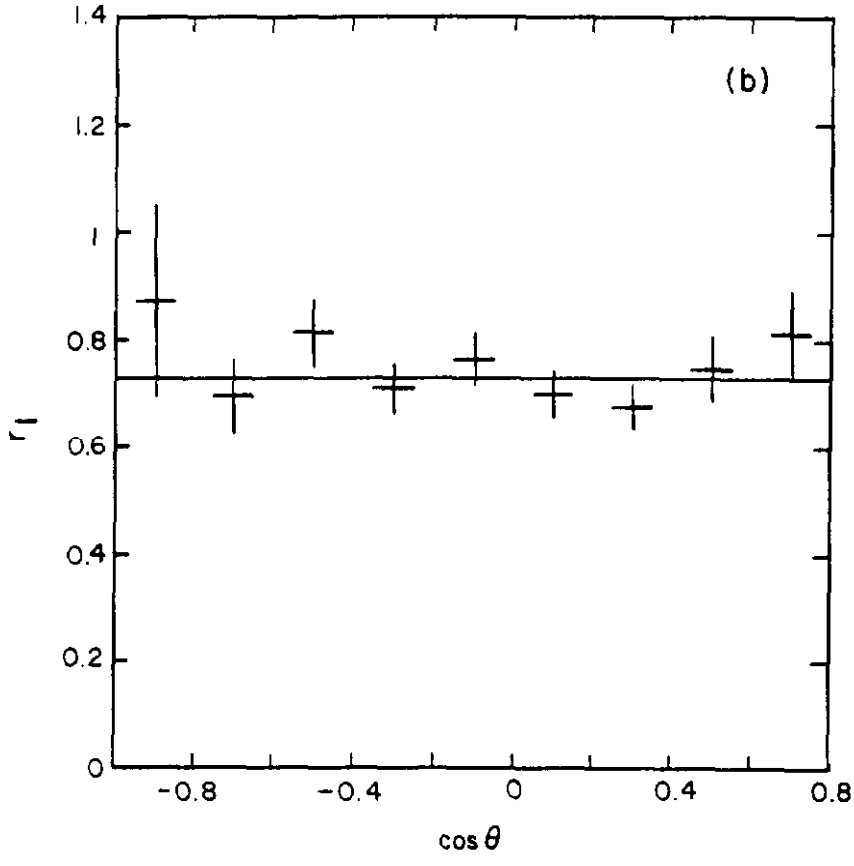

Figure 15b. Ratio of differential cross sections r_1 (see text) as a function of cosθ for this experiment's π^-W data.

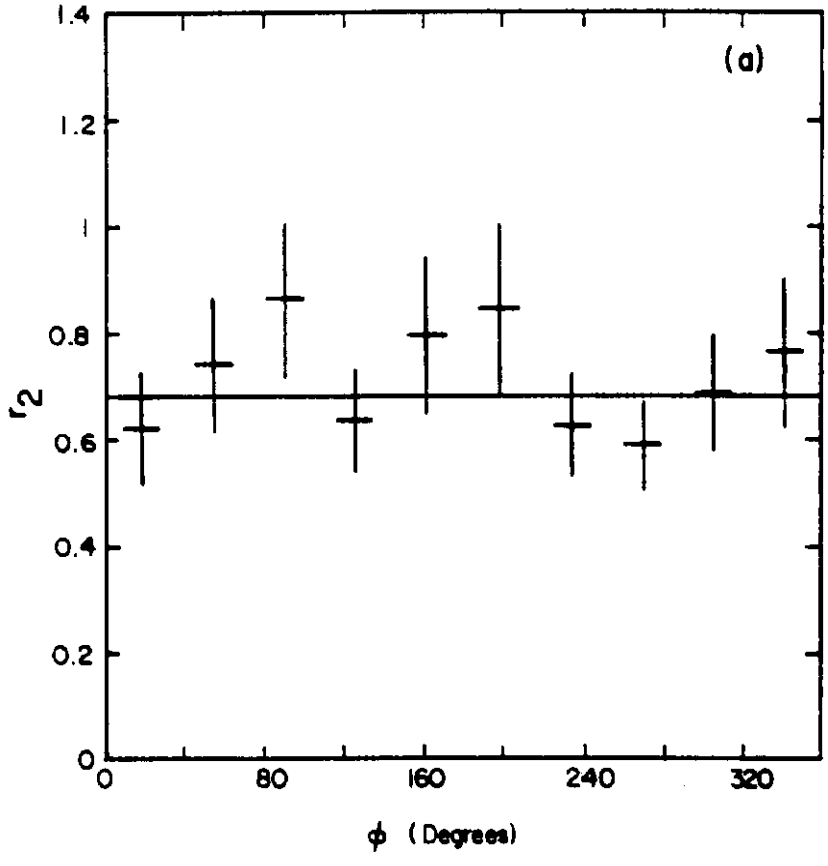

Figure 16a. Ratio of differential cross sections r_2 (see text) as a function of ϕ for this experiment's $\bar{p}W$ data.

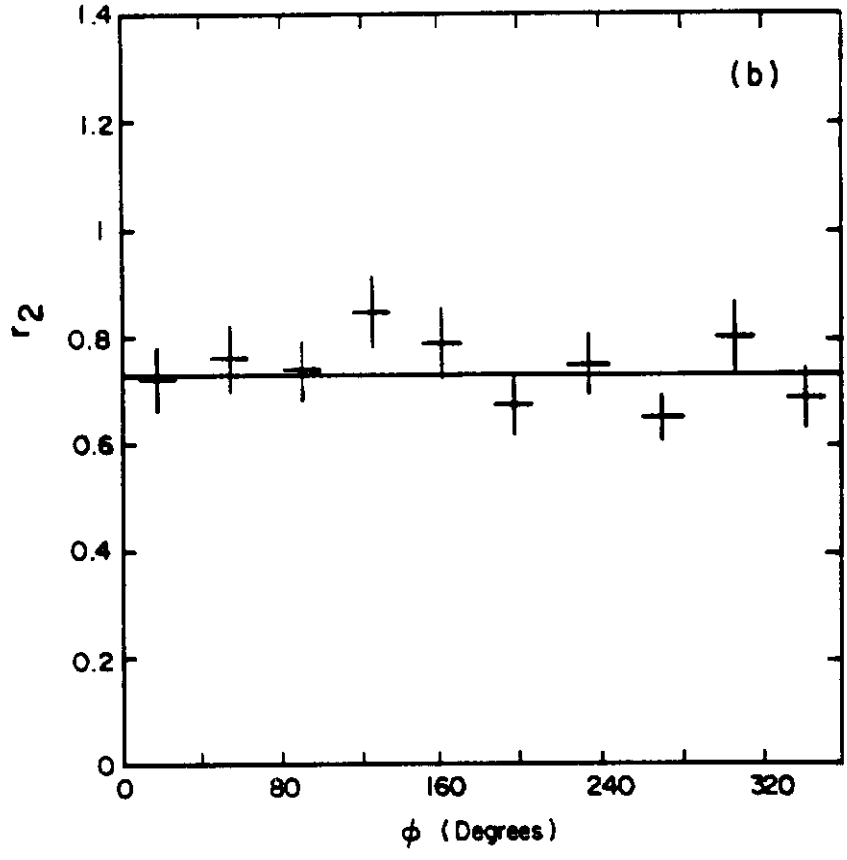

Figure 16b. Ratio of differential cross sections r_2 (see text) as a function of ϕ for this experiment's π^-W data.